

RESEARCH ARTICLE - FUNDAMENTAL

A multi-scale model of the coronary circulation applied to investigate transmural myocardial flow

Xinyang Ge^{1,2} | Zhaofang Yin³ | Yuqi Fan³ | Yuri Vassilevski^{4,5,6} | Fuyou Liang^{1,2,6} 

¹School of Naval Architecture, Ocean and Civil Engineering, Shanghai Jiao Tong University, Shanghai 200240, China

²Collaborative Innovation Center for Advanced Ship and Deep-Sea Exploration (CISSE), Shanghai Jiao Tong University, Shanghai 200240, China

³Department of Cardiology, Shanghai Ninth People's Hospital, Shanghai Jiao Tong University School of Medicine, Shanghai 200011, China

⁴Institute of Numerical Mathematics, Russian Academy of Sciences, Moscow 119333, Russia

⁵Moscow Institute of Physics and Technology, Dolgoprudny 141700, Russia

⁶Sechenov University, Moscow 119991, Russia

Correspondence

Fuyou Liang, School of Naval Architecture, Ocean and Civil Engineering, Shanghai Jiao Tong University, No.800 Dongchuan Road, Shanghai 200240, China.
Email: fuyouliang@sjtu.edu.cn

Funding information

National Natural Science Foundation of China, Grant/Award Number: 81611530715; SJTU Medical-Engineering Cross-cutting Research Foundation, Grant/Award Number: YG2016MS09; Russian Foundation for Basic Research, Grant/Award Number: 17-51-53160

Abstract

Distribution of blood flow in myocardium is a key determinant of the localization and severity of myocardial ischemia under impaired coronary perfusion conditions. Previous studies have extensively demonstrated the transmural difference of ischemic vulnerability. However, it remains incompletely understood how transmural myocardial flow is regulated under in vivo conditions. In the present study, a computational model of the coronary circulation was developed to quantitatively evaluate the sensitivity of transmural flow distribution to various cardiovascular and hemodynamic factors. The model was further incorporated with the flow autoregulatory mechanism to simulate the regulation of myocardial flow in the presence of coronary artery stenosis. Numerical tests demonstrated that heart rate (HR), intramyocardial tissue pressure (P_{im}), and coronary perfusion pressure (P_{per}) were the major determinant factors for transmural flow distribution (evaluated by the subendocardial-to-subepicardial (endo/epi) flow ratio) and that the flow autoregulatory mechanism played an important compensatory role in preserving subendocardial perfusion against reduced P_{per} . Further analysis for HR variation-induced hemodynamic changes revealed that the rise in endo/epi flow ratio accompanying HR decrease was attributable not only to the prolongation of cardiac diastole relative to systole, but more predominantly to the fall in P_{im} . Moreover, it was found that P_{im} and P_{per} interfered with each other with respect to their influence on transmural flow distribution. These results demonstrate the interactive effects of various cardiovascular and hemodynamic factors on transmural myocardial flow, highlighting the importance of taking into account patient-specific conditions in the explanation of clinical observations.

KEYWORDS

computational model, coronary circulation, flow autoregulation, transmural myocardial flow

1 | INTRODUCTION

Blood flow in the coronary circulation is highly heterogeneous and, in particular, transmural flow distribution in the myocardium is prone to the influence from multiple factors, such as coronary arterial pressure, myocardial stress, and the physiological or pathological state of intramyocardial vessels.¹⁻⁴ The patterns of transmural myocardial flow will be further complicated by the activation of compensatory mechanisms under ischemic conditions.⁵ In the diagnosis

of occlusive coronary artery disease, in addition to traditional angiographic evaluation of the severity of stenotic lesions in epicardial coronary arteries, attention has been increasingly paid to assessing the functional state of the coronary circulation with respect to, for example, coronary flow reserve, coronary flow capacity, microcirculatory resistance, myocardial flow reserve, and myocardial perfusion.⁶⁻¹¹ Accordingly, many new techniques have been developed and examined in various clinical settings.^{10,12-14} Despite the well-documented diagnostic utility of these new techniques, *in vivo* measurement of intramyocardial hemodynamic variables remains challenging, which largely hampers a thorough understanding of transmural myocardial flow. So far, techniques available to quantitatively measure myocardial blood flow have been applied mainly in animal experiments, such as electromagnetic flowmeter or myocardial contrast echocardiography used in combination with intravascular injection of radioactive microspheres or microbubbles.^{15,16} Animal experimental studies have revealed several important features of transmural myocardial flow, such as the vulnerability of subendocardium to ischemia¹⁷⁻²¹ and the reduction of the subendocardial-to-subepicardial (endo/epi) flow ratio following the increase in heart rate or the decrease in coronary perfusion pressure.^{18,22-24} Nevertheless, the measurement of flow rate in the myocardium alone is not sufficient to fully elucidate the mechanisms underlying the regulation of myocardial blood flow due to the lack of information on vascular state and mechanical stress in the myocardium.

In the scenario, computational modeling has emerged as a complementary approach to deepening the understanding of coronary hemodynamics. Models of the coronary circulation reported in the literature differed largely in form and degree of complexity, and have been applied to study various aspects of coronary hemodynamics, such as the effects of myocardial contraction on coronary flow waveform, pressure wave propagation in epicardial coronary arteries, and the interaction between coronary blood flow and myocardial mechanics or systemic hemodynamics.^{2,3,25-31} Relatively, only a limited number of model studies have been dedicated to investigating transmural myocardial flow.^{1,23,27,29,32-34} These studies not only confirmed the general findings of animal experiments, but also provided some new insights. For instance, higher compliance of vasculature in the subendocardium was demonstrated to be a causative factor for the redistribution of blood flow away from the subendocardium under reduced perfusion pressure conditions.¹ Pulmonary hypertension was found to have a substantial negative effect on blood flow in the right ventricular free wall and the rightmost layer of the ventricular septum.²⁹ Nonetheless, many aspects of transmural myocardial flow remain incompletely addressed, such as the interactive effects of cardiac and systemic hemodynamics on transmural distribution of myocardial flow, and the roles of the flow autoregulatory function of intramyocardial vessels in the regulation of transmural myocardial flow in the presence of coronary artery stenosis.

In the present study, we developed a multi-scale model of the coronary circulation capable of accounting for both cardiac-coronary-systemic hemodynamic interaction and coronary flow autoregulation, aiming to establish a practical numerical platform where the respective or combined effects of various cardiovascular/hemodynamic factors on transmural myocardial flow can be quantitatively investigated.

2 | METHODS

The coronary circulation was modeled as part of the entire cardiovascular system to account for the interaction between coronary blood flow and systemic hemodynamics (see Figure 1). Modeling of the cardiovascular system has been described in detail in a previous study,³⁵ where the systemic arteries were represented by a one-dimensional (1-D) model coupled with lumped-parameter (0-D) models of other cardiovascular portions. A similar modeling strategy was adopted to represent the coronary circulation, in which the large epicardial coronary arteries were represented by a 1-D model coupled with 0-D models of intramyocardial vessels (see Figure 1). Moreover, the flow autoregulatory function of coronary micro-vessels was mathematically modeled and incorporated into the hemodynamic model to enable the simulation of the regulatory behavior of coronary flow in the presence of coronary artery stenosis.

2.1 | One-dimensional modeling of the epicardial coronary arterial tree

The coronary arterial tree was assumed to be constituted by 87 large coronary arteries and 53 penetrating arteries (see Figure 1A) according to the anatomical data reported in Mynard and Smolich,²⁹ which was herein represented by a 1-D model to account for flow distribution and pulse wave propagation in epicardial coronary arteries. 1-D governing equations for blood flow in a coronary artery were the classical mass and momentum conservation equations.³⁵⁻³⁷

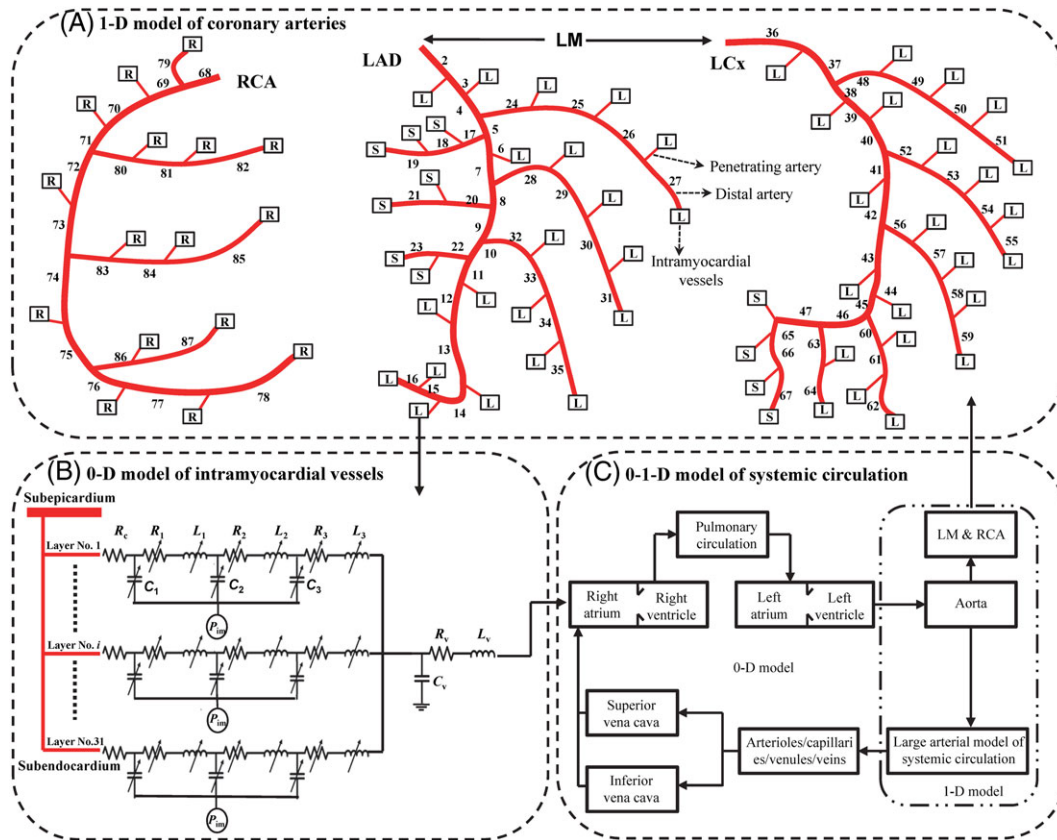


FIGURE 1 Schematic description of computational modeling of the coronary circulation coupled with the cardiovascular system. The 1-D model of the epicardial coronary arteries (Panel A) is coupled with the 0-1-D model of the cardiovascular system (Panel C) at the proximal ends and with the 0-D models of intramyocardial vessels (Panel B) at the distal ends. Each coronary arterial distal end is connected to an intramyocardial vascular subsystem that perfuses a specific myocardial district (denoted by the boxes in Panel A, with “L”, “R”, and “S” inside representing the left ventricular free wall, right ventricular free wall, and septum, respectively). Vessels in each intramyocardial vascular subsystem are distributed in multiple myocardial layers and represented by a series of variable resistances, compliances, and inductances to account for the effects of the time-varying and depth-dependent intramyocardial tissue pressure (P_{im}) on vascular deformation and blood flow. Blood flows through all intramyocardial vessels are directed via the coronary venous compartment to the right atrium to close the entire model system. Abbreviations: LM, left main coronary artery; LAD, left anterior descending artery; LCx, left circumflex artery; RCA, right coronary artery

$$\frac{\partial A}{\partial t} + \frac{\partial Q}{\partial z} = 0, \tag{1}$$

$$\frac{\partial Q}{\partial t} + \frac{\partial}{\partial z} \left(\gamma \frac{Q^2}{A} \right) + \frac{A \partial P}{\rho \partial z} + F_r \frac{Q}{A} = 0, \tag{2}$$

where t is the time, z the axial coordinate, and ρ the density of blood ($=1.06 \text{ g/cm}^3$); A , Q , and P denote the cross-sectional area, volume flux, and pressure, respectively; γ represents the momentum-flux correction coefficient and F_r the friction force per unit length, which were set to $4/3$ and $-8\pi\nu$, respectively, by assuming a Poiseuille cross-sectional velocity profile. The kinematic viscosity (ν) of blood was herein taken to be a constant value of $4.43 \text{ cm}^2/\text{s}$ based on the assumption that blood flows in medium to large sized arteries (eg, coronary arteries) behave like a Newtonian fluid.³⁸ The assumption has been widely adopted in previous modeling studies on arterial hemodynamics,^{28,37} and the predicted pressure distributions in the arterial system were comparable to those by non-Newtonian models.³⁹

To complete the system of Equations 1 and 2, a pressure-area relationship that accounts for the viscoelasticity of arterial wall was introduced.⁴⁰

$$P + \tau_\sigma \frac{\partial P}{\partial t} = \phi(A) + \tau_\epsilon \frac{\partial \phi(A)}{\partial t}, \quad \text{with } \phi(A) = \frac{Eh}{r_0(1-\sigma^2)} \left(\sqrt{\frac{A}{A_0}} - 1 \right) + P_0. \quad (3)$$

Here, A_0 and r_0 stand for the cross-sectional area and radius of artery at the reference pressure ($P_0 = 80$ mmHg), respectively. σ is the Poisson's ratio, herein taken to be 0.5 by assuming that the materials of vascular wall are incompressible. Eh/r_0 was firstly estimated based on the radius of artery according to the empirical formula proposed in Olufsen et al⁴¹ and subsequently modified to make the model-simulated pulse wave velocity (8.7 m/s) in the left anterior descending artery comparable to the measured data (8.6 ± 1.4 m/s).⁴² τ_σ and τ_ϵ are viscoelastic parameters representing the relaxation times for constant stress and strain, respectively, and they were herein estimated to be 0.01 and 0.017 seconds, respectively, giving a dynamic to static elastic modulus ratio of 1.7, a value close to that (1.83 ± 0.24) determined by in vitro experiments.⁴³ It is noted that by assigning fixed values to τ_σ and τ_ϵ , we actually neglected the frequency-dependent property of viscoelasticity.^{43,44} Nevertheless, compared with a purely elastic model, the viscoelastic model was effective in inhibiting unphysiological high-frequency oscillations when simulating coronary arterial pressure waves that are rapidly transmitted and repeatedly reflected between the aorta and coronary distal vessels.

For an artery with stenosis, Equations 1 and 2 are not sufficient to account for the energy loss resulting from the occurrence of flow recirculation or turbulence distal to the stenosis.⁴⁵ To handle the problem, an approach proposed in previous modeling studies^{46,47} was adopted, where the stenotic segment of an artery was isolated, with the pressure drop across it being represented by a lumped-parameter model established based on fluid dynamics experiments.⁴⁸

$$\Delta P = \frac{K_v \mu}{A_0 D_0} Q + \frac{K_t \rho}{2A_0^2} \left(\frac{A_0}{A_s} - 1 \right)^2 Q |Q| + \frac{K_u \rho L_s dQ}{A_0 dt}, \quad (4)$$

where ΔP and Q denote the pressure drop and flow rate through the stenotic segment, respectively; A_0/D_0 and A_s/D_s refer to the cross-sectional areas/diameters of the normal and stenotic arterial lumens, respectively; L_s is the stenosis length and μ the dynamic viscosity of blood (herein taken to be 0.0047 Pa.s). The three terms on the right-hand side of the equation represent pressure drops induced by viscous friction, energy loss due to flow turbulence in the expansion zone (immediately distal to the stenosis), and blood inertia, respectively. K_v , K_t , and K_u are empirical coefficients determined by experiments, with $K_v = 32 (0.83L_s + 1.64D_s) \times (A_0/A_s)^2/D_0$, $K_t = 1.52$ and $K_u = 1.2$, which have been proved to allow the predicted pressure drops by Equation 4 to match reasonably with measurements over a wide range of Reynolds numbers (100-1000)⁴⁹ that well covers the hemodynamic conditions in coronary arteries investigated in the present study. On the other hand, it should be noted that the lumped-parameter nature of Equation 4 makes it unable to describe pulse wave propagation within the stenotic segment. The stiffness of a stenosed arterial segment may differ considerably from that of a normal arterial segment due to the presence of atherosclerotic plaques,⁵⁰ which will generate impedance discontinuity, thereby inducing wave reflections at the proximal and distal ends of the stenosis. However, it has been suggested that impedance discontinuity at a stenosis is induced primarily by the increased viscous resistance and enhanced flow turbulence associated with an abrupt reduction in lumen area rather than the change in wall stiffness.⁵¹ In this sense, solving Equation 4 in conjunction with the 1-D model of normal arterial segments proximal and distal to a stenosis can be expected to reasonably account for wave reflections at the stenosis.

Continuity of mass flux and total blood pressure was imposed at all the arterial bifurcations to link hemodynamic variables in adjacent arteries.^{28,47,52} The proximal and distal ends of the coronary arterial tree were connected to the ascending aorta and intramyocardial vessels, respectively (see Figure 1).

2.2 | Lumped-parameter modeling of intramyocardial vessels

2.2.1 | Model configuration and governing equations

The epicardial coronary artery tree had in total 71 distal ends. We assumed that each distal end was connected to a cluster of intramyocardial vessels that perfuse a specific district of the myocardium. Due to the fact that the outerwalls of intramyocardial vessels are exposed to a tissue pressure that varies from epicardium to endocardium, intramyocardial vessels in each myocardial district were further distributed to multiple myocardial layers according to the penetration depth (see Figure 1B). It is noted that the number of myocardial layer division (N) was herein set to be 31, although previous studies usually adopted smaller layer division numbers ranging from one to eight.^{1,32,53,54} Our numerical tests

demonstrated that increasing the level of detail in layer division helped to stabilize the relationship between the effective and baseline resistances of intramyocardial vessels, thereby reducing the sensitivity of simulated coronary flow wave to an arbitrary choice of layer division number (see Appendix A for details). Vessels in each myocardial layer were further assembled into three series-arranged compartments (namely, arteriolar, capillary, and venular compartments), with each being represented by three lumped parameters that account for the viscous resistance to blood flow (R), compliance of vessel wall (C), and inertia of blood (L), respectively (see Figure 1B). Finally, venular flows in all myocardial layers were assumed to converge to a venous compartment through which coronary flow is directed to the right atrium. Blood flow through each vascular compartment was governed by the mass and momentum conservation equations as those generally adopted in previous studies.^{55,56} The governing equations of all vascular compartments formed a system of ordinary differential equations.

2.2.2 | Parameter settings

(1) Inter-layer distribution of baseline resistance and compliance

For each intramyocardial vascular subsystem connected to the distal end of an epicardial coronary artery, we assigned layer-specific vascular resistance and compliance on the basis of a prescribed total baseline (referring to the state of zero transvascular pressure) resistance (R_T) and compliance (C_T) of the vascular subsystem.

$$\begin{cases} R_T = \left(\sum_{n=1}^N \frac{1}{R_n} \right)^{-1} \\ C_T = \sum_{n=1}^N C_n \end{cases}, \quad (5)$$

$$R_n = \zeta R_N + (n-1) \left(\frac{1-\zeta}{N-1} \right) R_N, \quad (6)$$

$$C_n = C_T / N. \quad (7)$$

Here, R_n and C_n represent, respectively, the baseline vascular resistance and compliance in the n th myocardial layer, with N denoting the total number of layer division. We assumed that R_n varied among myocardial layers, while C_n distributed uniformly across the myocardium. ζ is a dimensionless coefficient used to adjust resistance allocation among myocardial layers so that the model-predicted endo/epi flow ratio under normal resting conditions is comparable to in vivo measurements. To adjust ζ , a linear negative feedback iterative approach was employed, which started from a pre-assigned initial value of ζ , with the relative difference (in percentage) between model-predicted and target endo/epi flow ratios being set as the objective function with a threshold value of 5%. In the present study, the target value of the endo/epi flow ratio in the left ventricular free wall was set to 1.30 based on previous in vivo measurements (1.14-1.50),⁵⁷⁻⁵⁹ leading to an optimized value of 2.2 for ζ , which was applied to set transmural resistance allocations in all myocardial walls.

The total baseline resistance (R_T) and compliance (C_T) of each intramyocardial vascular subsystem were assigned according to the anatomical connection of the afferent coronary artery to the proximal coronary artery trunks (ie, the left anterior descending artery [LAD], the left circumflex artery [LCx], and the right coronary artery [RCA]). We assumed that all intramyocardial vascular subsystems distal to a coronary artery trunk had a uniform R_T and C_T .

(1) Longitudinal allocation of vascular resistance and compliance in each myocardial layer

The allocation proportion of the baseline resistance among distal arteries (R_c), intramyocardial microvessels ($R_1 + R_2 + R_3$), and veins (R_v) (see Figure 1B for the locations of the resistances) was set to be 28%:65%:7% under normal resting conditions.⁶⁰ For intramyocardial microvessels, the resistance allocation proportion over arterioles, capillaries, and venules (ie, R_1 : R_2 : R_3) was estimated to be 60%:30%:10%, which allowed the simulated pre-capillary pressure drop (46 mmHg-55 mmHg) in the subepicardium of the left ventricular wall to agree with in vivo measurement (52 mmHg).⁶¹

The allocation proportion of baseline vascular compliance was set to be 9.5%:25.7%:31.4%:33.3% from distal arteries to veins (ie, $C_1:C_2:C_3:C_v$) based on the data reported in a previous study.⁵⁴

(2) Intramyocardial tissue pressure

Intramyocardial tissue pressure (P_{im}) is time-varying and dependent on both the contraction of the heart and the depth from the epicardium. Such characteristics were accounted for by defining P_{im} as the sum of the cavity-induced extracellular pressure (P_{CEP}) and the shortening-induced intramyocyte pressure (P_{SIP}).⁶²

$$P_{im} = \alpha P_{CEP} + P_{SIP}. \quad (8)$$

Herein, P_{CEP} was assumed to relate directly to the blood pressure in a cardiac chamber (P_{cbp}) and vary linearly from the subendocardium ($P_{CEP} = P_{cbp}$) to the subepicardium ($P_{CEP} = 0$). α is a coefficient (taken to be 1 by default) used to adjust the contribution of P_{cbp} to P_{im} . P_{SIP} was assumed to be proportional to the effective elastance of cardiac chamber.⁶²

$$P_{SIP} = \lambda E(t), \quad (9)$$

where E is a time-varying elastance that represents the systolic and diastolic function of a cardiac chamber (for details on the definition of E , please refer to Liang et al⁵⁶). λ was taken to be 7.0 mL so that peak P_{SIP} was approximately 18% of peak P_{CEP} for the left ventricle,²⁹ which fell in the range (10%-30%) determined by animal experiments.^{63,64} It is noted that the same value of λ was used for the right ventricle.

(3) Dependence of vascular resistance and compliance on vascular blood volume

The transvascular pressure (P_{tv}) of intramyocardial vessels, which is codetermined by intravascular blood pressure (P_b) and P_{im} (ie, $P_{tv} = P_b - P_{im}$), can vary over a wide range and induce marked changes in vascular lumen area, which in turn significantly alters vascular resistance and compliance. In this study, we related the resistance (R) and compliance (C) of each intramyocardial vascular compartment to the corresponding blood volume (V) based on the assumption that the lengths of intramyocardial vessels are constant despite changes in lumen area. In light of the resistance-lumen area relationship constructed for collapsible vessels in a previous study,⁶⁵ the resistance-volume (R - V) relationship was herein expressed as

$$R = G(V)R_0, \text{ with } G(V) = \begin{cases} a_c, & V \leq V_l; \\ \sum_{i=0}^3 a_i (V/V_0)^i, & V_l < V \leq V_0, \\ (V_0/V)^2, & V > V_0. \end{cases} \quad (10)$$

where R_0 refers to the baseline resistance at the reference blood volume (V_0) when vessel wall is free of transvascular pressure (= 0 Pa). V_l is the blood volume when opposite vascular walls start to contact under a negative transvascular pressure ($V_l = 0.21 V_0$). a_c, a_0, \dots, a_3 are scalar coefficients, which were taken to be 31.92, -0.91, 9.35, -12.99, and 5.55, respectively.⁶⁵ From Equation 10, the volume-dependent change of R can be divided into three stages: (1) when $V > V_0$, the R - V relationship follows from the Poiseuille's law; (2) when $V_l < V \leq V_0$, the R - V relationship is represented by a semi-analytical function constructed based on experimental data; and (3) when $V \leq V_l$, resistance is assumed to be constant because the contact of opposite vascular walls will provide additional force against transvascular pressure thus preventing a significant transvascular pressure-dependent change in vascular volume.

The C - V relationship was derived from the tube law applied to collapsible vessels.^{65,66}

$$C = \frac{C_0}{m_s - m_b} [m_s (V/V_0)^{m_s - 1} - m_b (V/V_0)^{m_b - 1}]^{-1}. \quad (11)$$

Here, C_0 refers to the baseline compliance at V_0 . The first and second terms on the right-hand side account for the changes of compliance with blood volume at positive and negative transvascular pressures, respectively, with m_s and m_b being coefficients that represent the mechanical properties of vessel wall under stretching and bending conditions,

respectively. m_b was set to be -1.5 for all types of vessels.⁶⁵ m_s was taken to be 1.0 for arteries and 10 for venules according to the values used in a previous study.⁶⁶ For capillaries, m_s was estimated to be 5 .

2.3 | Modeling of the autoregulatory mechanism of coronary flow

Coronary flow autoregulation reflects the intrinsic ability of coronary vessels to maintain an almost constant blood flow in the face of variations in perfusion pressure through myogenic, shear-dependent, and/or metabolic vasoresponses.⁶⁷ It has been observed in animal experiments that a sudden change in perfusion pressure induced an abrupt change in coronary arterial flow, but the altered coronary flow spontaneously returned to its original level in approximately 30 seconds to 2 minutes as a consequence of the rapid regulatory response of coronary micro-vessels.⁶⁸ On the other hand, the efficiency of flow autoregulation can be significantly compromised when perfusion pressure deviates largely from the physiological range, resulting in a nonlinear relationship between flow and perfusion pressure.⁶⁸ In the present study, we sought to simulate the stable hemodynamic state in the presence of coronary artery stenosis rather than reproduce the dynamic process of flow autoregulation subsequent to a sudden change in perfusion pressure. Therefore, the autoregulatory characteristic of coronary blood flow was herein accounted for by means of matching the results of model simulations with the steady-state relationship between coronary perfusion pressure and flow rate established in in vivo experiments. The coronary perfusion pressure-flow relationship (herein termed as the autoregulation curve) was derived by fitting a fourth-order polynomial function to available experimental data⁶⁸⁻⁷⁰ (see Figure 2). Because coronary flow autoregulation is mediated mainly by the vasoresponse of arterioles,⁷¹ the baseline vascular resistances in the intramyocardial arteriolar compartments of the model (ie, R_1 in Figure 1B) were automatically tuned via a proportional-integral-derivative feedback control loop to make the simulated pressure/flow pairs fall on the autoregulation curve. To facilitate numerical implementation, the proportional-integral-derivative feedback control of arteriolar resistance was expressed in a discrete form.

$$R^{k+1} = R^k \left[K_p \text{cor}(k) + K_i \sum_{j=0}^k \text{cor}(j) + K_d (\text{cor}(k) - \text{cor}(k-1)) \right], \quad (12)$$

$$\text{with } \text{cor}(k) = 1 + \frac{Q^k - Q^R}{Q^R}.$$

Here, R^k and R^{k+1} represent the arteriolar resistances at the k th and next iteration steps, respectively. $\text{cor}(k)$ is the correction function for R^k and is calculated based on the discrepancy between the simulated mean flow rate (Q^k) and the target value (Q^R , the mean flow rate corresponding to the simulated coronary perfusion pressure [P^k] on the autoregulation curve). K_p , K_i , and K_d are the gains, and their values were set, respectively, to be 1.2 , 0.01 , and 0.015 to allow rapid

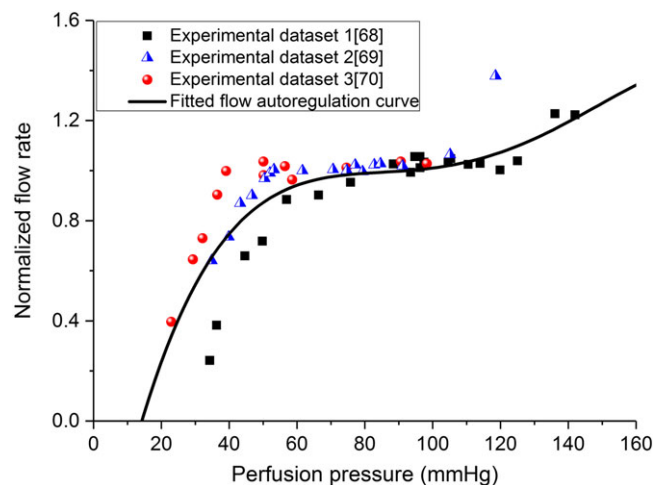


FIGURE 2 Relationship between coronary mean flow rate and perfusion pressure under in vivo conditions. All the flow rate data have been normalized by the flow rates measured at the reference perfusion pressures. The continuous line represents the coronary flow autoregulation curve obtained by fitting a fourth-order polynomial function to the experimental data⁶⁸⁻⁷⁰

convergence of the iteration computation. It is noted that the tuning of arteriolar resistance was implemented separately for each myocardial layer in consideration of the varying blood perfusion condition across the myocardium.

2.4 | Numerical methods

The 1-D partial differential equation system of the coronary arterial tree model and the 0-D ordinary differential equation system of the intramyocardial vascular models were merged into the equation systems of the global cardiovascular model and solved with the two-step Lax-Wendroff method and the fourth-order Runge-Kutta method, respectively. The solutions of the two equation systems were coupled at the model interfaces (ie, distal ends of the coronary arterial tree and the systemic arterial tree, and the inlet of the aorta) with an iterative method to ensure conservation of mass flux and momentum across the interfaces. More details on the numerical algorithms have been described elsewhere.⁴⁷

2.5 | Assignment of model parameters and model calibration

The parameters used in the models that represent the systemic portion of the cardiovascular system and the coronary arterial tree were derived from previous studies.^{29,35} Herein, the emphasis was placed on determining the values of parameters involved in the modeling of intramyocardial vessels.

A parameter tuning procedure was implemented to fit model solutions to available clinical data reported in the literature. The clinical data mainly included systemic arterial blood pressures, cardiac output, and mean flow rates in the three coronary artery trunks (ie, LAD, LCx, and RCA).^{72,73} These data have been measured in vivo under both normal resting and hyperemic conditions. Calibration of systemic arterial pressures and cardiac output was achieved mainly by tuning the total peripheral vascular resistance and total blood volume following from the methods adopted in Liang et al.^{56,74} It is noted that the contractility of the left and right ventricles was not determinable based on available clinical data and hence was maintained at its reference state (reported in Liang et al.³⁵) for the resting conditions, which was, however, elevated in proportion to heart rate to increase cardiac output under the hyperemic conditions. To calibrate model-predicted flow rates in the LAD, LCx, and RCA to in vivo measurements, the baseline resistances of intramyocardial vessels were tuned via a linear iteration algorithm, in which the relative difference (in percentage) between model-predicted and measured (target) flow rates is set as the objective function of parameter optimization. The algorithm operated iteratively in the following way until the criteria of convergence (ie, the value of the objective function is smaller than 1%) was reached: when the model-predicted flow rate was larger than the target value, the resistance was increased to reduce the flow rate, and vice versa. Because all intramyocardial vascular subsystems stemming from each of the three coronary artery trunks were assumed to have a uniform total resistance, the parameter tuning procedure involved only three resistance values despite the existence of 71 intramyocardial vascular subsystems. The resulting total baseline resistances of intramyocardial vascular subsystems distal to the LAD, LCx, and RCA were 78.53, 126.53, and 122.91 mmHg·s/mL, respectively, under the resting conditions, which were subsequently reduced to 20.54, 38.34, and 33.92 mmHg·s/mL, respectively to simulate increased coronary perfusion under the hyperemic conditions.

Table 1 shows that the model simulations agree reasonably with the in vivo measurements under both the resting and hyperemic conditions, demonstrating the ability of the model to simulate coronary hemodynamics over a wide

TABLE 1 Comparisons of model simulations with in vivo measurements under the normal resting and hyperemic conditions^{72,73}

	Baseline		Hyperemia	
	In vivo measurement	Simulation	In vivo measurement	Simulation
Heart rate (beats/min)	65.0 ± 8.0	66.0	96.00 ± 11.0	96.0
Systolic blood pressure (mmHg)	113.0 ± 5.0	113.0	113.00 ± 6.0	116.0
Diastolic blood pressure (mmHg)	74.0 ± 8.0	77.0	70.00 ± 5.0	69.0
Cardiac output (L/min)	5.19 ± 0.83	5.13	7.60 ± 1.19	7.50
LAD flow (mL/min)	76.15 ± 33.41	75.38	256.15 ± 110.84	258.21
LCx flow (mL/min)	54.62 ± 24.59	54.20	163.85 ± 67.18	162.02
RCA flow (mL/min)	68.46 ± 31.87	67.47	217.69 ± 76.70	215.17

range of physiological conditions. In addition to hemodynamic variables, the model-simulated deformation of subendocardial arterioles (herein quantified by the amplitude of the change in nominal diameter over a cardiac cycle calculated based on the simulated time history of arteriolar volume) was validated against in vivo measurements as well. If arterioles in the myocardial layers numbered from 21 to 31 are classified as subendocardial arterioles, the simulated amplitudes of nominal diameter change ranged from 22.5% to 37.3% (Figure 3), which agreed well with the measured data ($24 \pm 6\%$).⁷⁵

2.6 | Numerical tests

Three groups of numerical tests were carried out to address the following issues: (1) sensitivity of numerical solutions to model parameters or physiological factors; (2) coronary flow autoregulation in the presence of coronary artery stenosis; and (3) determinant factors for the distribution of transmural myocardial flow. In group (1), key parameters involved in the modeling of the coronary circulation and parameters representing the main properties of the cardiovascular system were varied by $\pm 25\%$ relative to their reference values to investigate their impacts on blood flow patterns in large coronary arteries and transmural flow distribution. In group (2), stenoses of various severities were introduced to an epicardial coronary artery to test the ability of the model to reproduce the autoregulatory phenomenon of coronary flow under reduced perfusion pressure conditions. In group (3), transmural myocardial flow was simulated under various physiological or pathological conditions to identify determinant factors for transmural flow distribution.

2.7 | Data analysis

General results of model simulations were reported in terms of the flow waves and their derivatives (eg, mean flow rate, diastolic flow proportion, mean diastolic/systolic flow velocity ratio) in the three coronary artery trunks (ie, LAD, LCx, and RCA). Given that the number of layer division was fixed at 31 when modeling each intramyocardial vascular system, layers No.1, No.16, and No.31 were assumed to represent vessels in the subepicardium, midwall, and subendocardium, respectively, with hemodynamic variables simulated in these layers being analyzed to investigate transmural myocardial flow. Accordingly, transmural flow distribution was evaluated quantitatively by the endo/epi flow ratio (calculated as the mean flow rate in myocardial layer No.31 divided by that in layer No.1). Moreover, when reporting simulated results related to transmural myocardial hemodynamics, by default, we refer to those in a myocardial district of the left ventricular free wall supplied by a branch artery (ie, artery No.27 in Figure 1A) of the LAD unless otherwise stated.

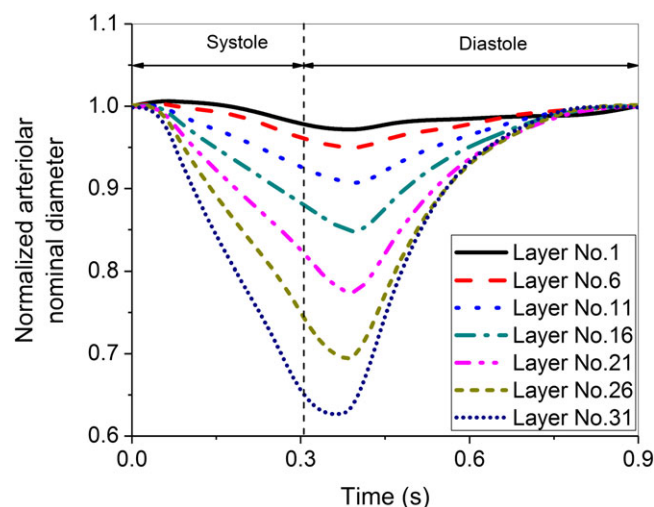


FIGURE 3 Time history of the changes in normalized nominal diameters of arterioles in different layers of the myocardial district supplied by a distal coronary artery (artery no. 27 in Figure 1A) under normal resting conditions. The nominal diameters are derived from the arteriolar volumes based on the assumption that the lengths of arterioles remain constant over a cardiac cycle, which are further normalized by the nominal diameters simulated at the beginning of systole to facilitate the evaluation of the amplitude of diameter change over a cardiac cycle

3 | RESULTS

3.1 | Coronary hemodynamics under normal resting and hyperemic conditions

Figure 4 shows the simulated flow waves in the three coronary artery trunks (ie, LAD, LCx, and RCA) under the normal resting and hyperemic conditions, respectively. The model predicted a typical biphasic flow waveform (characterized by diastolic dominance) in the LAD and LCx under the normal resting conditions (Figure 4A). By contrast, flow in the RCA was more evenly distributed over the cardiac cycle. These waveform features were basically consistent with previous in vivo observations.⁷⁶ Quantitatively, the simulated mean diastolic/systolic flow velocity ratio in the LAD was 1.88, which was close to the clinical data (1.8 ± 0.5) measured in patients with normal coronary perfusion.⁷⁷ Under the hyperemic conditions, in addition to a marked increase in total blood flow rate through the coronary arteries, there were significant changes in flow waveform, such as the increased peak flow in systole (see Figure 4B), which agreed qualitatively with clinical observations.^{78,79}

Figure 5 shows the simulated arteriolar/venular flow waveforms in three representative myocardial layers (ie, layers No.1, No.16 and No.31) supplied by a distal coronary artery (artery No.27 in Figure 1A). The arteriolar flow waveform was diastolic dominant (see Figure 5A), with the degree (indicated by the diastolic flow proportion) increasing from the subepicardium towards the subendocardium. By contrast, the venular flow waveform was characterized by a dominant flow portion in systole (see Figure 5C), which reasonably reproduced the flow characteristics measured in the great cardiac vein.⁸⁰ The layer-specific characteristics of flow waveform were maintained under the hyperemic conditions (see Figure 5B,D), although there were some changes in the shape of flow waveform due to the changes in heart rate and coronary vascular resistance. Moreover, the simulated endo/epi flow ratio (1.30) under the normal resting conditions agreed well with in vivo measurements (1.14-1.50),⁵⁷⁻⁵⁹ and did not change significantly under the hyperemic conditions ($1.30 \rightarrow 1.38$) as was observed in animal experiments.⁵⁷

3.2 | Parameter sensitivity analysis

Numerical tests were carried out to investigate the sensitivity of coronary flow patterns to physiological or model parameters. The physiological parameters were those representing the major cardiovascular properties or physiological states, including the total vascular resistance (R_{cor}) and compliance (C_{cor}) of the coronary circulation, the total peripheral vascular resistance (R_{sys}), Young's modulus (stiffness) of the aorta (E_{aor}), the systolic function (E_{lva}) and diastolic function (E_{lva}) of the left ventricle, and heart rate (HR). The model parameters mainly included those involved in the modeling of the coronary circulation, such as α (in Equation 8), λ (in Equation 9), ζ (in Equation 6), and m_s and m_b (in Equation 11). In the sensitivity analysis study, each parameter was varied by $\pm 25\%$ relative to its default value. The changes in coronary flow in response to parameter variations were evaluated with respect to three hemodynamic indices, namely, the mean LAD flow rate (Q_{LAD}), the mean diastolic/systolic flow velocity ratio (V_{dia}/V_{sys}) in the LAD, and the endo/epi flow ratio (Q_{endo}/Q_{epi}) in a myocardial district supplied by the LAD. To facilitate inter-parameter comparison, the simulated

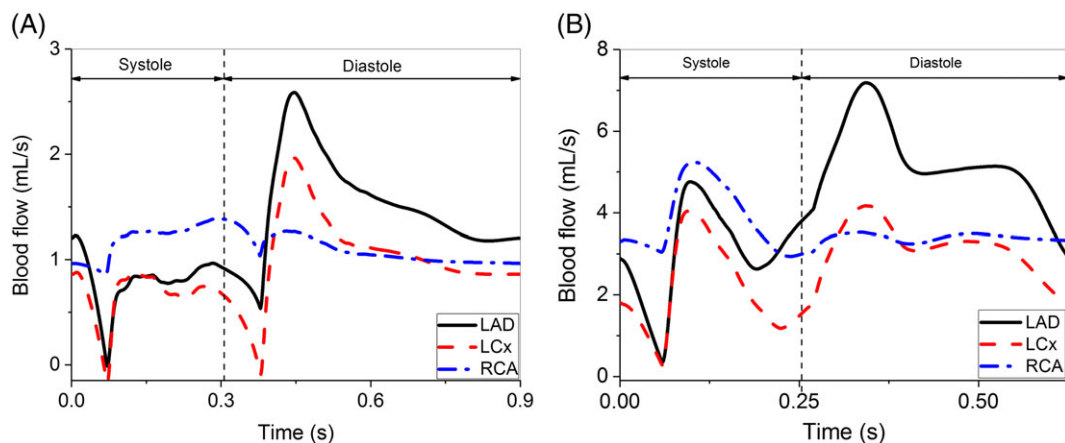


FIGURE 4 Simulated blood flow waves in the LAD, LCx, and RCA under normal resting (A) and hyperemic (B) conditions. Herein, the systole and diastole of a cardiac cycle are divided according to the elastance curve of the left ventricle (eg, systole starts at the onset of elastance increase and ends when the elastance reaches the maximum)

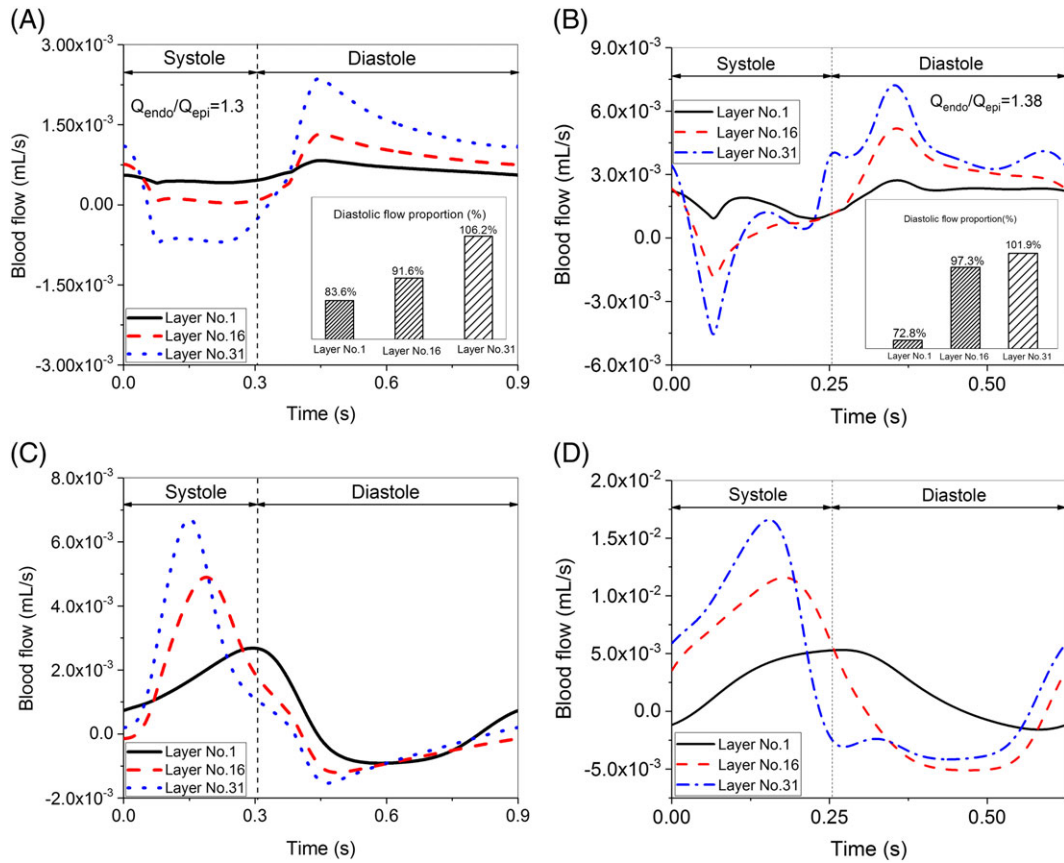


FIGURE 5 Simulated arteriolar (A, B) and venular (C, D) flow waves in the subepicardium (layer no. 1), midwall (layer no. 16), and subendocardium (layer no. 31) of a myocardial district of the left ventricular free wall supplied by a distal coronary artery (artery no. 27 in Figure 1A) under normal resting and hyperemic conditions. The embedded graphs illustrate the layer-specific proportion of diastolic flow to total flow over a cardiac cycle. Q_{endo}/Q_{epi} represents the endo/epi flow ratio

changes in hemodynamic indices were expressed in form of percentage changes relative to the values computed under the reference conditions (normal resting conditions corresponding to the data reported in Table 1). Obtained results are summarized in Table 2. It was observed that Q_{LAD} was dominated by R_{cor} and considerably influenced by R_{sys} ; Q_{endo}/Q_{epi} was highly sensitive to ζ , followed by α and HR ; and V_{dia}/V_{sys} was influenced significantly by HR , C_{cor} , and α , and moderately by λ and R_{cor} .

TABLE 2 Sensitivities of model solutions to major physiological and model parameters. The sensitivity indices are expressed in the form of percentage changes in LAD mean flow rate (Q_{LAD}), endo/epi flow ratio in the left ventricular free wall (Q_{endo}/Q_{epi}), and mean diastolic/systolic flow velocity ratio in the LAD (V_{dia}/V_{sys}) relative to the default values (simulated under the normal resting conditions). Please see the text for the details of parameter notation

	Parameter Variation	Q_{LAD}	Q_{endo}/Q_{epi}	V_{dia}/V_{sys}
Physiological parameters	R_{cor}	+25%/−25%	−20.0/32.0	−3.10/2.38
	R_{sys}	+25%/−25%	20.0/−23.0	1.08/−2.24
	C_{cor}	+25%/−25%	−0.17/0.29	−2.69/2.12
	E_{Iva}	+25%/−25%	2.7/−4.7	0.35/−0.5
	E_{Ivb}	+25%/−25%	−5.9/6.8	−0.91/0.38
	HR	+25%/−25%	6.6/−8.5	−8.62/4.73
	E_{aor}	+25%/−25%	−0.043/0.07	−0.25/0.1
	Model parameters	α	+25%/−25%	−4.6/5.9
λ		+25%/−25%	−2.2/2.4	0.40/−0.44
ζ		+25%/−25%	−0.76/0.9	21.94/−23.09
m_s		+25%/−25%	−0.88/0.99	1.15/−1.31
m_b		+25%/−25%	0.59/−0.53	0.78/−1.15

The three hemodynamic indices differed considerably with respect to the specific parameters to which they are sensitive, due to their differences in characterizing coronary hemodynamics. For instance, Q_{LAD} reflects the overall amount of blood perfusion to the myocardium, which is, as expected, determined primarily by the resistance of coronary vessels (R_{cor}) and the perfusion pressure (ie, aortic pressure determined mainly by the systemic vascular resistance [R_{sys}]). Q_{endo}/Q_{epi} , as an index of transmural myocardial flow distribution, is affected directly by transmural vascular resistance allocation (controlled by ζ according to Equation 6), and indirectly by the intramyocardial tissue pressure (determined mainly by α and HR) via its influence on the dynamic relationships between baseline and effective coronary vascular resistances in different myocardial layers (according to Equation 10). V_{dia}/V_{sys} , as a measure of the relative perfusion proportion in diastole vs. systole over a cardiac cycle, is not only affected evidently by the proportion of diastole in a cardiac cycle as determined by HR , but also is strongly sensitive to α and C_{cor} because these parameters significantly affect the effective resistance of intramyocardial vessels during systole via their respective influences on intramyocardial tissue pressure and the relationship between effective and baseline vascular resistances. These results provided useful insights for understanding the dynamics of coronary blood flow and its associations with various physiological or pathological factors. In the present study, because we were interested mainly in the transmural distribution of coronary blood flow, subsequent numerical tests will focus on Q_{endo}/Q_{epi} .

3.3 | Coronary flow autoregulation in the presence of coronary artery stenosis

A stenosis (with a length of 5 mm) was created in the mid LAD (artery No.9 in Figure 1A), with its severity (represented by diameter stenosis rate) being increased from 0% to 80% to produce various degrees of reduced coronary perfusion pressure. Under each condition, simulations were performed with and without the incorporation of the flow autoregulatory mechanism, respectively, to highlight the role of flow autoregulation. Figure 6A shows the simulated mean flow rate plotted against the perfusion pressure distal to the stenosis. With the incorporation of the flow autoregulatory mechanism, as expected, the model-simulated data points fell exactly on the autoregulation curve; whereas, the simulated flow rates exhibited a strong dependence on perfusion pressure if the flow autoregulatory mechanism was removed. The amount of flow compensation by the autoregulatory mechanism increased progressively with the increase in stenosis severity until reaching a maximum at a stenosis rate of 66%; thereafter, the effect of flow compensation steeply diminished following a further increase in stenosis severity (see Figure 6B).

3.4 | Determinant factors for transmural flow distribution

In this study, the endo/epi flow ratio (monitored in the myocardial district supplied by coronary artery No.27 illustrated in Figure 1A) was used to characterize transmural flow distribution in the left ventricular free wall. Based on the results of parameter sensitivity analysis, three parameters (ie, α , ζ , and HR) were selected for further sensitivity analysis. Here, α is a major determinant of intramyocardial tissue pressure given the blood pressure in the left ventricle, ζ controls the

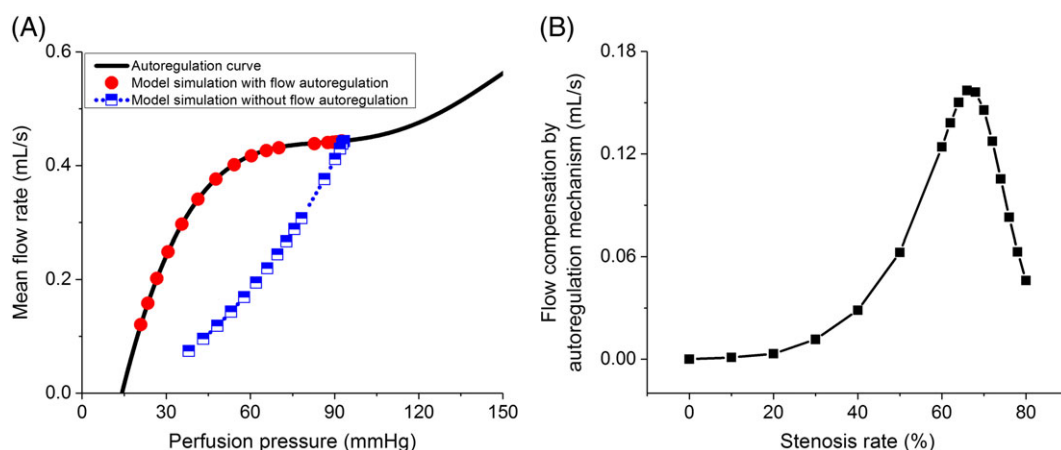


FIGURE 6 Simulated flow-pressure relationship distal to a stenosis in the mid LAD (artery no. 9 in Figure 1A) with and without flow autoregulation compared against the flow autoregulation curve (solid line) (A), and the amount of flow compensation by flow autoregulation (B). The diameter stenosis rate is varied from 0% to 80%. The amount of flow compensation is plotted against the stenosis rate to illustrate its sensitivity to stenotic condition

allocation of vascular resistance among myocardial layers, and HR is a factor affecting global hemodynamics. Additional to the previously mentioned three parameters, R_{cor} , m_b , and E_{aor} , which represent the vascular properties in the coronary and systemic circulations (R_{cor} : tone of intramyocardial vessels, m_b : bending stiffness of intramyocardial vessels, E_{aor} : stiffness of the aorta), were included as well. Each parameter was varied from -50% to $+50\%$ relative to the default value at an interval of 10% . It is noted that the coronary flow autoregulatory mechanism has been removed to highlight the influence of each individual parameter. In line with the results of parameter sensitivity analysis as reported in Table 2, Figure 7A shows that the endo/epi flow ratio is sensitive most strongly to α , ζ , and HR . By contrast, varying R_{cor} , m_b , and E_{aor} only had mild influences. Figure 7B shows the endo/epi ratios of the effective vascular resistance (ie, coronary arterial-to-venous pressure gradient divided by mean flow rate) corresponding to -50% and $+50\%$ parameter variations, respectively. The pronounced changes in endo/epi ratio of the effective vascular resistance can reasonably account for the strong sensitivity of endo/epi flow ratio to the variations in α and ζ given the fact that coronary perfusion pressure is almost not affected by varying the parameters. The change in endo/epi ratio of the effective vascular resistance with HR was, however, moderate, implying that there might be other mechanisms underlying the strong sensitivity of endo/epi flow ratio to the variation in HR .

To further explore the mechanisms by which HR variation affects transmural flow distribution, the model of the coronary circulation was decoupled from the systemic model so that the intramyocardial tissue pressure (P_{im}) and coronary perfusion pressure (P_{per}), which are dependent on HR under in vivo conditions, could be separately defined in numerical tests. Herein, sensitivity analysis for HR was re-performed with the decoupled coronary circulation model under three conditions: (1) constant mean P_{im} (fixed at the mean P_{im} [=44.3 mmHg] computed at default HR [66 beats/minute]) and HR -dependent P_{per} ; (2) constant mean P_{per} (fixed at the mean P_{per} [=92.3 mmHg] computed at default HR) and HR -dependent P_{im} ; and (3) constant mean P_{im} and P_{per} ($P_{im} = 44.3$ mmHg and $P_{per} = 92.3$ mmHg). The obtained results are compared with those computed for the intact condition (ie, P_{im} and P_{per} vary physiologically with HR) in Figure 8A. It is evident that with constant P_{im} and/or P_{per} the sensitivity of endo/epi flow ratio to variations in HR differs significantly from that simulated for the intact condition. To further quantitatively explore the mechanisms behind the phenomenon, the independent contribution of HR variation to the change in endo/epi flow ratio was firstly evaluated by calculating the amount of change in endo/epi flow ratio over the range of HR variation with constant P_{im} and P_{per} , which was then subtracted from the simulated changes in endo/epi flow ratio with constant P_{im} or P_{per} , thereby obtaining a quantitative evaluation of the respective contributions of P_{per} and P_{im} . The corresponding results are plotted in Figure 8B. The physiological decrease in P_{im} (from 55.6 mmHg to 29.9 mmHg) accompanying the decrease of HR (from $+50\%$ to -50%) was found to be a major contributor to the increase in endo/epi flow ratio, although the decrease in HR per se did play a role of elevating the endo/epi flow ratio. By contrast, the fall in P_{per} (from 103.2 mmHg to 76.0 mmHg) accompanying HR decrease was observed to reduce the endo/epi flow ratio.

The decoupled coronary circulation model was further utilized to investigate the response of endo/epi flow ratio to simultaneous variations in P_{im} and P_{per} (relative to the reference values) at a fixed HR (66 beats/minute). Obtained results (see Figure 9A for the surface plot and Figure 9B for the contour lines projected on the $P_{im} - P_{per}$ plane) showed

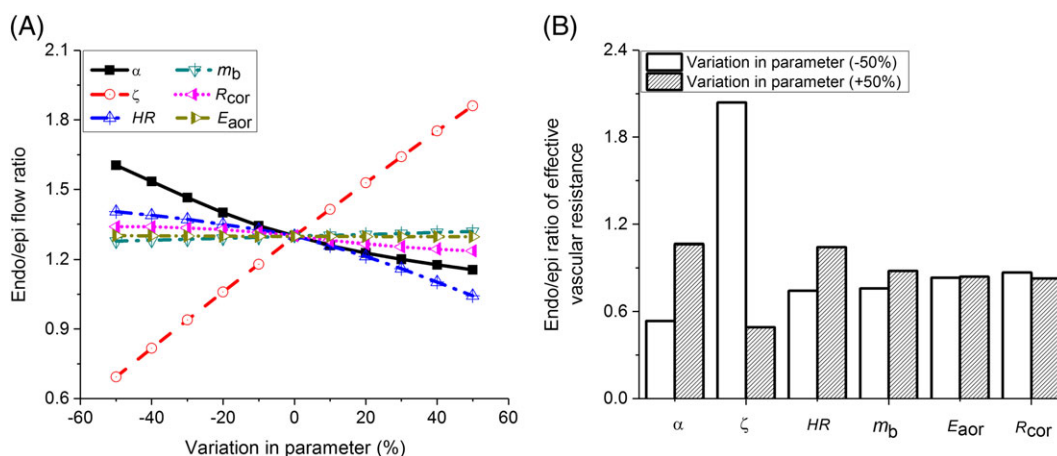


FIGURE 7 Changes in endo/epi flow ratio (in the myocardial district supplied by a distal coronary artery [artery no. 27 in Figure 1A]) in response to variations in physiological and model parameters (from -50% to $+50\%$ relative to the default value at an interval of 10%) (A), and the endo/epi ratios of effective vascular resistance (coronary arterial-to-venous pressure gradient divided by mean flow rate) corresponding to -50% and $+50\%$ variations in parameters, respectively (B)

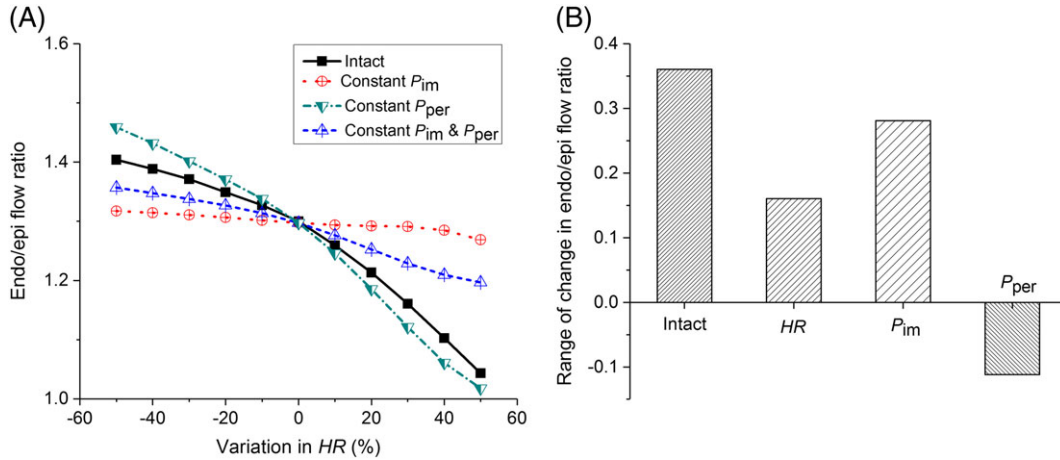


FIGURE 8 Changes in endo/epi flow ratio (in the myocardial district supplied by a distal coronary artery [artery no. 27 in Figure 1A]) with HR under controlled coronary perfusion pressure (P_{per}) and intramyocardial tissue pressure (P_{im}) conditions (A), and the respective contributions of HR, P_{per} , and P_{im} to the change in endo/epi flow ratio over the range of HR variation (from +50% to -50%) (B). Please see the text for more details on the simulation conditions

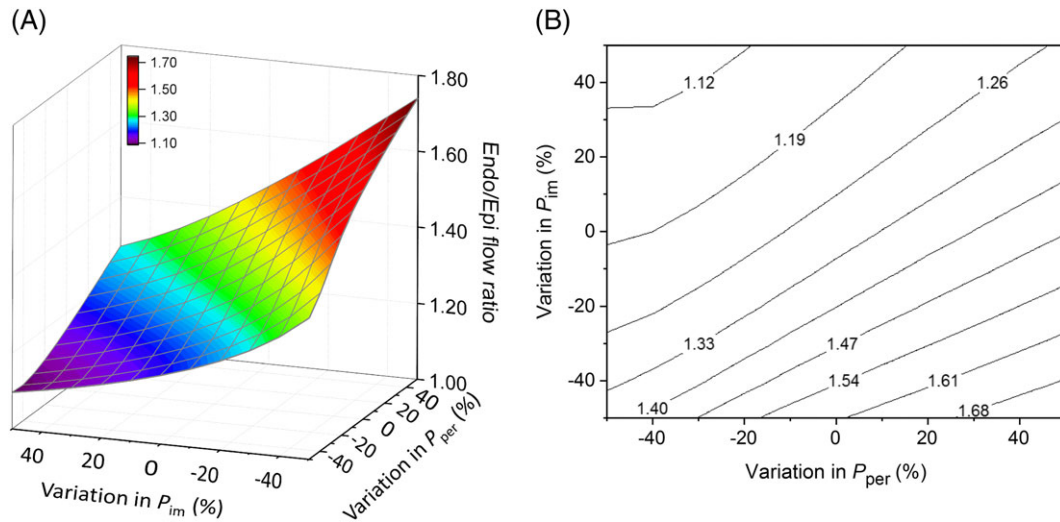


FIGURE 9 Distributions of endo/epi flow ratio (in the myocardial district supplied by a distal coronary artery [artery no. 27 in Figure 1A]) corresponding to different combinations of P_{per} and P_{im} (represented by percentage variations relative to their reference values). Panel (A) is the surface plot and Panel (B) is the contour lines obtained by projecting the surface plot on the $P_{per} - P_{im}$ plane. Note that HR was fixed at 66 beats/minute, and the flow autoregulation mechanism was not incorporated in the simulations

that the range of changes in endo/epi flow ratio induced by varying P_{im} was wider when P_{per} was high, and, on the other hand, the sensitivity of endo/epi flow ratio to variations in P_{per} was stronger with a low P_{im} than with a high P_{im} . These results indicate that there exists a considerable interaction effect between P_{im} and P_{per} with respect to their influence on transmural flow distribution.

3.5 | Influence of coronary flow autoregulation on transmural flow distribution

To test the influence of coronary flow autoregulation on transmural flow distribution, a stenosis was created in one of the branch arteries of the LAD (ie, artery No.27 in Figure 1A) to produce various perfusion pressures by increasing the stenosis rate from 0% up to 80%. Figure 10A shows the simulated mean flow rates (relative values normalized by the reference flow rates) in three representative myocardial layers (ie, No.1, No.16, and No.31) plotted against the mean coronary arterial pressure distal to the stenosis. The simulated flow rates in all the three layers strictly complied with the autoregulation curve when the perfusion pressure was higher than 46 mmHg but started to deviate as the perfusion

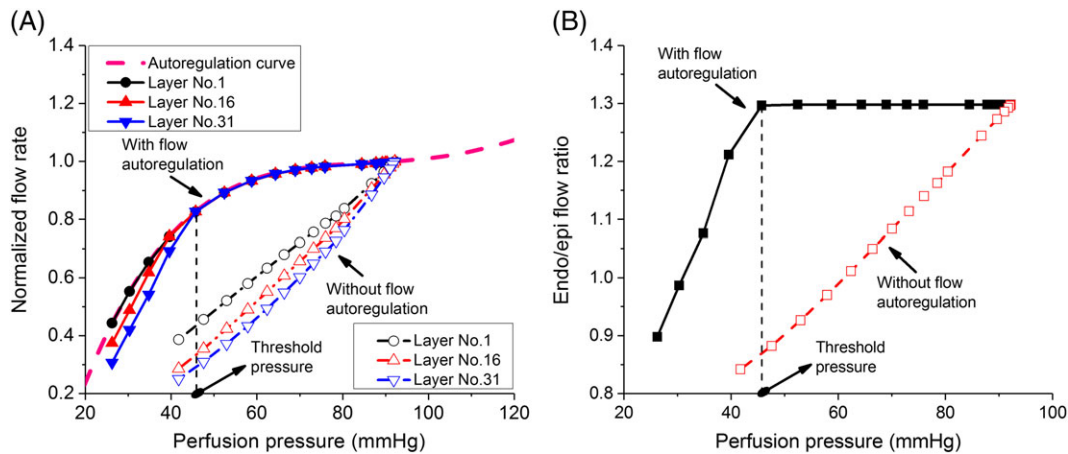


FIGURE 10 Changes in mean flow rates in different myocardial layers (A) and endo/epi flow ratio (B) with the perfusion pressure distal to a stenosis in a distal coronary artery (artery no. 27 in Figure 1A). The plotted flow rate in each myocardial layer has been normalized by the flow rate simulated for the normal perfusion pressure to facilitate inter-layer comparison. The severity of the stenosis is varied from 0% to 80% to generate different levels of perfusion pressure. The simulated results with and without the incorporation of flow autoregulation are both plotted to highlight the effect of flow autoregulation on transmural flow distribution. The threshold pressure denotes the pressure at which the subendocardial flow starts to deviate from the autoregulation curve and the endo/epi flow ratio becomes dependent on perfusion pressure following a further decrease in perfusion pressure

pressure fell further, with the flow rate in the subendocardium exhibiting the highest sensitivity to the perfusion pressure (exhibiting a nearly linear relationship between flow rate and perfusion pressure). Correspondingly, Figure 10B shows that the endo/epi flow ratio is maintained constant despite the decrease in perfusion pressure when the perfusion pressure is higher than the threshold value (46 mmHg), but steeply decreases with further fall in perfusion pressure. To more clearly highlight the role of flow autoregulation in preserving the endo/epi flow ratio, Figure 10 also illustrates the simulated results in the absence of flow autoregulation. Evidently, both the flow rate and the endo/epi flow ratio decreased almost linearly with the fall of coronary perfusion pressure after the flow autoregulatory mechanism was removed.

4 | DISCUSSION

4.1 | Contributions in model development

A computational model of the coronary circulation was developed to investigate the sensitivity of transmural myocardial flow to various cardiovascular and hemodynamic factors. The model simulations reasonably reproduced the hemodynamic data measured under both normal resting and hyperemic conditions. In comparison with similar models reported in the literature, major improvements of the present work consist in three aspects: (1) a more detailed hierarchical modeling of intramyocardial vessels, (2) a more sophisticated representation of the nonlinear relationships between vascular resistance/compliance and vascular volume, and (3) the incorporation of the coronary flow autoregulatory mechanism in the simulation of transmural myocardial flow.

When representing the complex anatomical configuration of intramyocardial coronary vessels, previous studies adopted a variety of layer-division strategies based on empirical assumptions, with the number of layer division ranging from one to eight.^{27,32,62,81,82} However, few studies addressed whether the outcomes of model simulation are sensitive to layer division. Our study demonstrated that the simulated coronary artery flow wave changed considerably with variations in layer division despite the fixed total baseline resistance of intramyocardial vessels (see Figure A1 in Appendix A). The phenomenon was dominated by the layer division-dependent relationship between the effective and baseline resistances of intramyocardial vessels. Following the increase in layer division number, a stable effective-baseline resistance relationship was gradually established. Therefore, adopting a large layer division number was expected to attenuate the sensitivity of numerical results to an arbitrary choice of layer division number, which would facilitate model parameter assignment given that the baseline resistance of intramyocardial vessels can be derived from perfusion experiments on arrested hearts.

A major improvement in the representation of the dynamic deformation and associated hemodynamic effects of intramyocardial vessels is the introduction of a piecewise function to account for the nonlinear relationship between vascular resistance and volume. Different from previous studies^{27,62} where a Poiseuille volume-resistance relationship was adopted regardless of the mechanical state of vascular wall, our study adopted the Poiseuille volume-resistance relationship only when the vascular wall was stretched by a positive transvascular pressure (ie, $V > V_0$). When the transvascular pressure went down to a negative value (ie, $V < V_0$), a semi-analytical formula was adopted instead because the vascular wall bore bending force and deformed inward in a non-circular shape, making the Poiseuille law no longer applicative. Accordingly, the vascular compliance was modeled as a function of vascular volume by taking into account both the bending and stretching stiffness of vascular wall. These formulations enabled the model to simulate the deformation and associated hemodynamic effects of intramyocardial vessels over a wide range of transvascular pressure. The simulated amplitudes of the changes in nominal diameters of arterioles over a cardiac cycle (22.5%~37.3%) in the subendocardium of the left ventricular free wall agreed reasonably with the in vivo measurements ($24 \pm 6\%$),⁷⁵ partly proving the ability of our model to simulate the in vivo deformation of intramyocardial vessels.

Flow autoregulation is an inherent physiological function of intramyocardial vessels that plays a crucial role in maintaining myocardial perfusion upon variations in coronary perfusion pressure. Previous studies have developed some models capable of simulating the dynamic responses of coronary flow to sudden changes in coronary perfusion pressure,^{83,84} but did not address the regulatory behaviors of transmural myocardial flow. The transmural characteristics of flow autoregulation have been addressed in a model-based study.³³ The study, however, focused on the effects of diastolic time fraction on flow autoregulatory function and utilized an oversimplified model that ignored the dynamic deformation of intramyocardial vessels and coronary-systemic hemodynamic interaction. In the present study, incorporating the flow autoregulatory mechanism into a more detailed hemodynamic model of the coronary circulation enabled us to further address the transmural characteristics of vascular and hemodynamic responses to varying perfusion pressure. With the model, we, in addition to confirming the general role of the flow autoregulatory mechanism in preserving myocardial perfusion, demonstrated the dependence of the compensatory efficiency of flow autoregulation on the severity of coronary artery stenosis. For instance, the amount of flow compensation was found to be largest in the presence of a moderate rather than severe coronary artery stenosis (see Figure 6B). Moreover, our study revealed that the threshold of flow autoregulation was firstly reached in the subendocardium when coronary perfusion pressure decreased lower than 46 mmHg (close to that [=50 mmHg] determined by animal experiments¹⁵), which could partly explain why the subendocardium is more vulnerable to ischemia in the presence of severe coronary artery stenosis.^{18,22}

Overall, the present model offers a reasonable tool for simulating hemodynamic variables both in large epicardial coronary arteries and intramyocardial vessels under various physiological or pathological conditions.

4.2 | Insights into determinant factors for transmural flow distribution

Our numerical study revealed that transmural flow distribution in the left ventricular free wall was influenced mainly by transmural allocation of vascular resistance (controlled by ζ in the model), HR , intramyocardial tissue pressure (P_{im}), and coronary perfusion pressure (P_{per}). The influence of transmural vascular resistance allocation can be readily inferred from general hemodynamic knowledge. Therefore, our discussion will focus on the latter three factors. From the results of numerical tests, increasing HR , elevating P_{im} , and reducing P_{per} led to remarkable blood flow redistribution away from the subendocardium, which is basically consistent with the findings reported in previous computational^{1,27,32,33} and experimental studies.^{5,18-20,22-24,34} New insights from our study are as follows: (1) the observed effect on transmural flow distribution of HR variation is codetermined by multiple factors, (2) P_{im} and P_{per} interact with each other with respect to their influence on transmural flow distribution, and (3) the flow autoregulatory function of intramyocardial vessels significantly reduces the sensitivity of endo/epi flow ratio to P_{per} .

Decreasing HR per se moderately increases the endo/epi flow ratio because the prolongation of cardiac diastole relative to systole favors subendocardial perfusion which is dependent more strongly on the low P_{im} period in a cardiac cycle (relating directly to the duration of diastole) than subepicardial perfusion (see Figure 5A). Physiologically, P_{im} and P_{per} are dependent hemodynamic variables of HR . No previous studies have quantitatively investigated their respective contributions to transmural flow distribution in the context of HR variation. Our study revealed that the falls in P_{im} and P_{per} accompanying HR decrease have opposite effects on transmural flow distribution, with the former contributing even largely than the increase in cardiac diastole/systole ratio to the elevation of endo/epi flow ratio, while the later

reducing endo/epi flow ratio (see Figure 8B). Moreover, from the results presented in Figure 9, given the same degree of variation, P_{im} induced a larger change in endo/epi flow ratio than P_{per} , implying that P_{im} is more powerful than P_{per} in affecting transmural flow distribution. On the other hand, the sensitivity of endo/epi flow ratio to P_{im} was affected by the status of P_{per} , and vice versa. For instance, the efficiency of reducing P_{im} to improve endo/epi flow ratio was higher with a higher P_{per} , whereas the degree of elevation in endo/epi flow ratio associated with an increase in P_{per} was larger in the presence of a lower P_{im} . These findings underline the importance of taking into account multiple hemodynamic factors for a comprehensive understanding of transmural myocardial flow.

The important role of the flow autoregulatory mechanism in preserving coronary arterial flow against a varying coronary perfusion pressure has been extensively demonstrated by *in vivo* studies.⁶⁸⁻⁷⁰ However, none of these studies gave a detailed investigation on the influence of flow autoregulation on transmural flow distribution. Our study demonstrated that in the presence of coronary flow autoregulation the endo/epi flow ratio was preserved over a wide range of coronary perfusion pressure (see Figure 10B), which is basically consistent with the observations of a previous *in vivo* study on dogs⁸⁵ although the study did not specifically address the role of coronary flow autoregulation. Furthermore, our study revealed that the role of flow autoregulation in maintaining endo/epi flow ratio was significantly compromised when coronary perfusion pressure fell lower than a threshold value of 46 mmHg. The mechanism behind the phenomenon is that microvessels in the subendocardium must dilate to a larger extent than those in the subepicardium to preserve endo/epi flow ratio upon a decrease in perfusion pressure, which leads the vasodilation potential of micro-vessels in the subendocardium to exhaust early during a progressive decrease in perfusion pressure.

4.3 | Clinical implications

Many medications (eg, beta-blockers, calcium-channel blockers) have been found to be efficacious in reducing the size of myocardial perfusion defects or relieving clinical symptoms.⁸⁶ However, mechanistic interpretations for clinical observations were usually speculative due to technical limitations of *in vivo* measurements. For instance, despite the well-known *HR*/blood pressure lowering effect of beta-blockers,⁸⁷ no clinical studies were able to elucidate how such medication-induced hemodynamic changes contribute exactly to the improvement in myocardial perfusion. A recent *in silico* study suggested that the reduction in systemic arterial pressure, decrease in left ventricular work, and increase in coronary flow contributed to the cardioprotective efficiency of beta-blockers.⁸⁸ Our study further demonstrated the beneficial role of *HR* decrease in improving subendocardial perfusion. In the meantime, our results revealed that the fall in P_{im} secondary to *HR* decrease contributed more significantly to the elevation of endo/epi flow ratio and that the lowering of arterial blood pressure actually played a counteractive role by reducing endo/epi flow ratio. These results imply that knowledge of the systemic hemodynamic responses to a certain medication is necessary for a better understanding of its effects on myocardial perfusion, especially in view of the fact that medication-induced hemodynamic changes not only depend on the type of drugs but also differ among patients.⁸⁹

The finding regarding the interactive role of P_{im} and P_{per} in regulating endo/epi flow ratio may have clinical implications under certain pathological conditions, particularly under the condition that the flow autoregulatory function of intramyocardial vessels is largely exhausted by severe ischemic challenge. For instance, for patients with extremely high P_{im} and low P_{per} , (eg, in the presence of severe aortic valve stenosis), elevating P_{per} may not be an effective approach to improving subendocardial perfusion. Similarly, for patients with a severely lowered P_{per} (eg, in the presence of severe coronary arterial stenosis), reducing P_{im} will not bring a significant improvement in subendocardial perfusion as can be expected with a normal P_{per} .

In patients with coronary microvascular dysfunction, impaired myogenic function (ie, elevated minimal vascular resistance at maximal dilation, which is a major determinant of the threshold of flow autoregulation) can significantly compromise the compensatory performance of intramyocardial vessels,⁹⁰⁻⁹² thus increasing the susceptibility of subendocardium to ischemia in the presence of coronary arterial stenosis. For such patients, normalization of the coronary vascular myogenic function might be expected to improve the tolerance to coronary arterial stenotic disease.

4.4 | Limitations and future works

Major limitations of the study consist in two aspects: (1) the omission of coronary collateral vessels, and (2) the fixed flow autoregulation curve for vessels in different myocardial layers. Collateral flow is a common feature of myocardial flow under ischemic conditions.⁹³ It has been extensively demonstrated that coronary anastomoses with a collateral

function exist in both normal and diseased coronary circulation and, in particular, collateral vessels may grow to strengthen the compensatory role of collateral flow against impaired proximal perfusion in chronic coronary artery disease.⁹⁴ In this sense, including collateral vessels in the modeling of the coronary circulation could be expected to improve the fidelity of myocardial flow simulation under ischemic conditions. However, given the fact that the location and anatomy of collateral vessels are highly patient specific and prone to dynamic changes following the progression of coronary artery disease, it is currently difficult to construct a model that is representative of the collateral vessels in the general population and applicable to various pathophysiological conditions. For this reason, coronary collateral vessels have been omitted in the present study, which may to some extent lead to an overestimation of ischemia in the subendocardium, but would not alter the general findings regarding the relationships between transmural flow distribution and various cardiovascular/hemodynamic factors.

The coronary flow autoregulation curve has been constructed based on the experimental data collected from the literature and applied to all myocardial layers. However, coronary flow autoregulation has been found to shift upward in hypertensive patients with ventricular hypertrophy,⁹⁵ which implies that the relationship between perfusion pressure and flow is subject to dynamic changes under the long-term influence of mechanical and hemodynamic disorders in the myocardium. In chronic coronary artery disease, the varying ischemic potential across the myocardium might elicit myocardial depth-dependent vascular remodeling and modulation of vascular tone, ultimately forming layer-specific flow autoregulation curves. Therefore, applying an identical flow autoregulation curve across the entire myocardium might cause the model predictions to deviate from in vivo conditions. Although the model-predicted threshold pressure of flow autoregulation in subendocardium is close to that measured in short-term (in a time scale of minutes) ischemic experiments,¹⁵ it remains unclear whether the model is sufficient to predict transmural flow in the context of long-term (in a time scale of months or years) ischemia. In future studies, inclusion of coronary collateral vessels and adoption of layer-specific flow autoregulation curves would be expected to further improve the predictive power of the model, although support of sufficient in vivo data is required.

5 | CONCLUSIONS

The study presented a computational model of the coronary circulation capable of not only simulating coronary hemodynamics under various pathophysiological conditions but also quantifying the effects of various cardiovascular/hemodynamic factors on transmural myocardial flow. The results demonstrated the different contributions of multiple factors associated with *HR* variation to transmural flow redistribution, the interaction between intramyocardial tissue pressure and coronary perfusion pressure with respect to their influence on the endo/epi flow ratio, and the important role of coronary flow autoregulation in preserving a physiological endo/epi flow ratio over a wide range of coronary perfusion pressure. These findings may serve as useful theoretical references for explaining clinical observations.

ACKNOWLEDGEMENT

The study was supported by the National Natural Science Foundation of China (Grant no. 81611530715) and the SJTU Medical-Engineering Cross-cutting Research Foundation (Grant no. YG2016MS09). Yuri Vassilevski was supported by the Russian Foundation for Basic Research (Grant no. 17-51-53160).

CONFLICT OF INTEREST STATEMENT

None declared.

ORCID

Fuyou Liang  <http://orcid.org/0000-0001-5012-486X>

REFERENCES

1. Algranati D, Kassab GS, Lanir Y. Why is the subendocardium more vulnerable to ischemia? A new paradigm. *Am J Physiol Heart & Circulatory Phys Ther.* 2011;300(3):H1090-H1100.

2. Huo Y, Kassab GS. A hybrid one-dimensional/Womersley model of pulsatile blood flow in the entire coronary arterial tree. *Ajp Heart & Circulatory Phys Ther.* 2007;292(292):H2623-H2633.
3. Smith NP. A computational study of the interaction between coronary blood flow and myocardial mechanics. *Physiol Meas.* 2004;25(4):863-877.
4. Bache RJ, Cobb FR, Jr GJ. Myocardial blood flow distribution during ischemia-induced coronary vasodilation in the unanesthetized dog. *J Clin Investig.* 1974;54(6):1462-1472.
5. Merkus D, Vergroesen I, Hiramatsu O, Tachibana H, Nakamoto H, sToyota E, Goto M, Ogasawara Y, Spaan JA, Kajiya F.. Stenosis differentially affects subendocardial and subepicardial arterioles in vivo. *Am J Physiol Heart & Circulatory Phys Ther* 2001;280(4):H1674-H1682.
6. Layland J, Nerlekar N, Palmer S, Berry C, Oldroyd K. Invasive assessment of the coronary microcirculation in the catheter laboratory. *Int J Cardiol.* 2015;199:141-149.
7. Lee BK, Lim HS, Fearon WF, et al. Invasive evaluation of patients with angina in the absence of obstructive coronary artery disease. *Circulation.* 2015;131(1):61-62.
8. Melikian N, De Bondt P, Tonino P, et al. Fractional flow reserve and myocardial perfusion imaging in patients with angiographic multivessel coronary artery disease. *JACC Cardiovasc Interv.* 2010;3(3):307-314.
9. Schuijf JD, Wijns W, Jukema JW, et al. Relationship between noninvasive coronary angiography with multi-slice computed tomography and myocardial perfusion imaging. *J Am Coll Cardiol.* 2006;48(12):2508-2514.
10. van de Hoef TP, Echavarría-Pinto M, van Lavieren MA, et al. Diagnostic and prognostic implications of coronary flow capacity: a comprehensive cross-modality physiological concept in ischemic heart disease. *JACC Cardiovasc Interv.* 2015;8(13):1670-1680.
11. Klein R, Hung GU, Wu TC, et al. Feasibility and operator variability of myocardial blood flow and reserve measurements with Tc-99m-sestamibi quantitative dynamic SPECT/CT imaging. *J Nucl Cardiol.* 2014;21(6):1075-1088.
12. Nagel E, Klein C, Paetsch I, et al. Magnetic resonance perfusion measurements for the noninvasive detection of coronary artery disease. *Circulation.* 2003;108(4):432-437.
13. Tonino PA, De Bruyne B, Pijls NH, et al. Fractional flow reserve versus angiography for guiding percutaneous coronary intervention. *N Engl J Med.* 2009;360(3):213-224.
14. van de Hoef TP, Siebes M, Spaan JA, Piek JJ. Fundamentals in clinical coronary physiology: why coronary flow is more important than coronary pressure. 2015;36(47):3312-3319.
15. Weintraub WS, Hattori S, Agarwal JB, Bodenheimer MM, Banka VS, Helfant RH. The relationship between myocardial blood flow and contraction by myocardial layer in the canine left ventricle during ischemia. *Circ Res.* 1981;48(3):430-438.
16. Wei K, Jayaweera AR, Firoozan S, Linka A, Skyba DM, Kaul S. Quantification of myocardial blood flow with ultrasound-induced destruction of microbubbles administered as a constant venous infusion. *Circulation.* 1998;97(5):473-483.
17. Hoffman JI. Why is myocardial ischaemia so commonly subendocardial? *Clin Sci.* 1981;61(6):657-662.
18. Bache RJ, Schwartz JS. Effect of perfusion pressure distal to a coronary stenosis on transmural myocardial blood flow. *Circulation.* 1982;65(5):928-935.
19. Bache RJ, Cobb FR. Effect of maximal coronary vasodilation on transmural myocardial perfusion during tachycardia in the awake dog. *Circ Res.* 1977;41(5):648-653.
20. Domenech RJ, Goich J. Effect of heart rate on regional coronary blood flow. *Cardiovasc Res.* 1976;10(2):224-231.
21. Goto M, Flynn AE, Doucette JW, et al. Cardiac contraction affects deep myocardial vessels predominantly. *Am J Physiol.* 1991;261(5 Pt 2): H1417-H1429.
22. Hoffman JI et al. Determinants and prediction of transmural myocardial perfusion. *Circulation.* 1978;58(3 Pt 1):381-391.
23. Flynn AE, Coggins DL, Goto M, et al. Does systolic subepicardial perfusion come from retrograde subendocardial flow? *Am J Physiol.* 1992;262(2):1759-1769.
24. Fokkema DS, VanTeeffelen JW, Dekker S, Vergroesen I, Reitsma JB, Spaan JA. Diastolic time fraction as a determinant of subendocardial perfusion. *Am J Physiol Heart & Circulatory Phys Ther.* 2005;288(5):H2450-H2456.
25. Downey JM, Kirk ES. Inhibition of coronary blood flow by a vascular waterfall mechanism. *Circ Res.* 1975;36(6):753-760.
26. Spaan JA, Cornelissen AJ, Chan C, Dankelman J, Yin FC. Dynamics of flow, resistance, and intramural vascular volume in canine coronary circulation. *Ajp Heart & Circulatory Physiol.* 2000;278(2):H383-H403.
27. Algranati D, Kassab GY. Mechanisms of myocardium-coronary vessel interaction. *Am J Physiol.* 2010;298(2):861-873.
28. Mynard JP, Nithiarasu P. A 1D arterial blood flow model incorporating ventricular pressure, aortic valve and regional coronary flow using the locally conservative Galerkin (LCG) method. *Int J Numeric Methods Biomed Eng.* 2008;24(5):367-417.
29. Mynard JP, Smolich JJ. Influence of anatomical dominance and hypertension on coronary conduit arterial and microcirculatory flow patterns: a multiscale modeling study. *Am J Physiol Heart Circ Physiol.* 2016;311(1):H11-H23.

30. van der Horst A, Boogaard FL, van't Veer M, Rutten MC, Pijls NH, van de Vosse FN. Towards patient-specific modeling of coronary hemodynamics in healthy and diseased state. *Comput Math Methods Med*. 2013;2013(6). 393792
31. Zhao X, Liu Y, Li L, Wang W, Xie J, Zhao Z. Hemodynamics of the string phenomenon in the internal thoracic artery grafted to the left anterior descending artery with moderate stenosis. *J Biomech*. 2015;49(7):983-991.
32. Bruinsma P, Arts T, Dankelman J, Spaan JA. Model of the coronary circulation based on pressure dependence of coronary resistance and compliance. *Basic Res Cardiol*. 1988;83(5):510-524.
33. van den Wijngaard JP, Kolyva C, Siebes M, et al. Model prediction of subendocardial perfusion of the coronary circulation in the presence of an epicardial coronary artery stenosis. *Med Biol Eng Comput*. 2008;46(5):421-432.
34. Chadwick RS, Tedgui A, Michel JB, Ohayon J, Levy BI. Phasic regional myocardial inflow and outflow: comparison of theory and experiments. *Am J Physiol*. 1990;258(2):1687-1698.
35. Liang FY, Takagi S, Himeno R, Liu H. Biomechanical characterization of ventricular-arterial coupling during aging: a multi-scale model study. *J Biomech*. 2009;42(6):692-704.
36. Blanco PJ, Watanabe SM, Dari EA, Passos MA, Feijóo RA. Blood flow distribution in an anatomically detailed arterial network model: criteria and algorithms. *Biomech Model Mechanobiol*. 2014;13(6):1303-1330.
37. Formaggia L, Lamponi D, Tuveri M, Veneziani A. Numerical modeling of 1D arterial networks coupled with a lumped parameters description of the heart. *Comput Methods Biomech Biomed Engin*. 2006;9(5):273-288.
38. Ku DN. Blood flow in arteries. *Annu Rev Fluid Mech*. 1997;29(1):399-434.
39. Reymond P, Perren F, Lazeyras F, Stergiopoulos N. Patient-specific mean pressure drop in the systemic arterial tree, a comparison between 1-D and 3-D models. *J Biomech*. 2012;45(15):2499-2505.
40. Guan D, Liang F, Gremaud PA. Comparison of the Windkessel model and structured-tree model applied to prescribe outflow boundary conditions for a one-dimensional arterial tree model. *J Biomech*. 2016;49(9):1583-1592.
41. Olufsen MS, Peskin CS, Kim WY, Pedersen EM, Nadim A, Larsen J. Numerical simulation and experimental validation of blood flow in arteries with structured-tree outflow conditions. *Ann Biomed Eng*. 2000;28(11):1281-1299.
42. Arts T, Kruger RT, van Gerven W, Lambregts JA, Reneman RS. Propagation velocity and reflection of pressure waves in the canine coronary artery. *Am J Physiol*. 1979;237(4):H469-H474.
43. Gow BS, Hadfield CD. The elasticity of canine and human coronary arteries with reference to postmortem changes. *Circ Res*. 1979;45(5):588-594.
44. Holzapfel GA, Gasser TC, Stadler M. A structural model for the viscoelastic behavior of arterial walls: continuum formulation and finite element analysis. *Eur J Mechan*. 2002;21(3):441-463.
45. Oliveira PJ, Pinho FT. Pressure drop coefficient of laminar Newtonian flow in axisymmetric sudden expansions. *Int J Heat & Fluid Flow*. 1997;18(5):518-529.
46. Stergiopoulos N, Young DF, Rogge TR. Computer simulation of arterial flow with applications to arterial and aortic stenoses. *J Biomech*. 1992;25(12):1477-1488.
47. Liang F, Takagi S, Himeno R, Liu H. Multi-scale modeling of the human cardiovascular system with applications to aortic valvular and arterial stenoses. *Med Biol Eng Comput*. 2009;47(7):743-755.
48. Young DF, Tsai FY. Flow characteristics in models of arterial stenoses. II. Unsteady flow. *J Biomech*. 1973;6(5):547-559.
49. Seeley BD, Young DF. Effect of geometry on pressure losses across models of arterial stenoses. *J Biomech*. 1976;9(7):439-446.
50. Claridge MW, Bate GR, Hoskins PR, Adam DJ, Bradbury AW, Wilmsink AB. Measurement of arterial stiffness in subjects with vascular disease: are vessel wall changes more sensitive than increase in intima-media thickness? *Atherosclerosis*. 2009;205(2):477-480.
51. Farrar DJ, Green HD, Peterson DW. Noninvasively and invasively measured pulsatile haemodynamics with graded arterial stenosis. *Cardiovasc Res*. 1979;13(1):45-57.
52. Müller LO, Toro EF. A global multiscale mathematical model for the human circulation with emphasis on the venous system. *Int J Num Methods Biomed Eng*. 2014;30(7):681-725.
53. Mynard JP, Smolich JJ. One-dimensional haemodynamic modeling and wave dynamics in the entire adult circulation. *Ann Biomed Eng*. 2015;43(6):1443-1460.
54. Spaan JA. Coronary diastolic pressure-flow relation and zero flow pressure explained on the basis of intramyocardial compliance. *Circ Res*. 1985;56(3):293-309.
55. Alastruey J, Parker KH, Peiró J, Sherwin SJ. Lumped parameter outflow models for 1-D blood flow simulations: effect on pulse waves and parameter estimation. *Comm Computation Phys*. 2006;4(2):317-336.
56. Liang F, Senzaki H, Kurishima C, Sughimoto K, Inuzuka R, Liu H. Hemodynamic performance of the Fontan circulation compared with a normal biventricular circulation: a computational model study. *Am J Physiol Heart & Circulatory Phys Ther*. 2014;307(7):H1056-H1072.

57. Crystal GJ, Downey HF, Bashour FA. Small vessel and total coronary blood volume during intracoronary adenosine. *Am J Physiol.* 1981;241(2):194-201.
58. Domenech RJ. Regional diastolic coronary blood flow during diastolic ventricular hypertension. *Cardiovasc Res.* 1978;12(11):639-645.
59. Weiss HR, Winbury MM. Nitroglycerin and chromonar on small-vessel blood content of the ventricular walls. *Am J Physiol.* 1974;226(4):838-843.
60. Bovendeerd PH, Borsje P, Arts T, van De Vosse FN. Dependence of intramyocardial pressure and coronary flow on ventricular loading and contractility: a model study. *Ann Biomed Eng.* 2006;34(12):1833-1845.
61. Chilian WM, Eastham CL, Marcus ML. Microvascular distribution of coronary vascular resistance in beating left ventricle. *Am J Physiol.* 1986;251(2):779-788.
62. Mynard JP, Penny DJ, Smolich JJ. Scalability and in vivo validation of a multiscale numerical model of the left coronary circulation. *Am J Physiol Heart Circ Physiol.* 2014;306(4):H517-H528.
63. Mihalescu LS, Abel FL. Intramyocardial pressure gradients in working and nonworking isolated cat hearts. *Am J Physiol.* 1994;266(3 Pt 2):H1233-H1241.
64. Rabbany SY, Kresh JY, Noordergraaf A. Intramyocardial pressure: interaction of myocardial fluid pressure and fiber stress. *Am J Physiol.* 1989;257(2 Pt 2):H357-H364.
65. Fullana JM, Zaleski S. A branched one-dimensional model of vessel networks. *J Fluid Mech.* 2009;621(621):183-204.
66. Marchandise E, Flaud P. Accurate modelling of unsteady flows in collapsible tubes. *Comput Methods Biomech Biomed Engin.* 2010;13(2):279-290.
67. Waters SL, Alastruey J, Beard DA, et al. Theoretical models for coronary vascular biomechanics: progress & challenges. *Prog Biophys Mol Biol.* 2011;104(1-3):49-76.
68. Mosher P, Ross J Jr, Mcfate PA, Shaw RF. Control of coronary blood flow by an autoregulatory mechanism. *Circ Res.* 1964;14(3):250-259.
69. Rouleau J, Boerboom LE, Surjadhana A, Hoffman JI. The role of autoregulation and tissue diastolic pressures in the transmural distribution of left ventricular blood flow in anesthetized dogs. *Circ Res.* 1979;45(6):804-815.
70. Jr ST, Jr CJ. Modulation of coronary autoregulatory responses by nitric oxide. Evidence for flow-dependent resistance adjustments in conscious dogs. *Circ Res.* 1993;73(2):232-240.
71. Kanatsuka H, Lamping KG, Eastham CL, Marcus ML. Heterogeneous changes in epimyocardial microvascular size during graded coronary stenosis. Evidence of the microvascular site for autoregulation. *Circ Res.* 1990;66(2):389-396.
72. Watzinger N, Lund GK, Saeed M, et al. Myocardial blood flow in patients with dilated cardiomyopathy: quantitative assessment with velocity-encoded cine magnetic resonance imaging of the coronary sinus. *J Magnet Res Imaging JMRI.* 2005;41(6):347-353.
73. Wieneke H, von Birgelen C, Haude M, et al. Determinants of coronary blood flow in humans: quantification by intracoronary Doppler and ultrasound. *J Appl Physiol.* 2005;98(3):1076-1082.
74. Liang F, Oshima M, Huang H, Liu H, Takagi S. Numerical study of cerebroarterial hemodynamic changes following carotid artery operation: a comparison between multiscale modeling and stand-alone three-dimensional modeling. *J Biomech Eng.* 2015;137(10):101011.
75. Yada T, Hiramatsu O, Kimura A, et al. In vivo observation of subendocardial microvessels of the beating porcine heart using a needle-probe videomicroscope with a CCD camera. *Circ Res.* 1993;72(5):939-946.
76. Skolidis EI, Kochiadakis GE, Koukouraki SI, Parthenakis FI, Karkavitsas NS, Vardas PE. Phasic coronary flow pattern and flow reserve in patients with left bundle branch block and normal coronary arteries. *J Am Coll Cardiol.* 1999;33(5):1338-1346.
77. Segal J, Kern MJ, Scott NA, et al. Alterations of phasic coronary artery flow velocity humans during percutaneous coronary angioplasty. *J Am Coll Cardiol.* 1992;20(2):276-286.
78. Daimon M, Watanabe H, Yamagishi H, et al. Physiologic assessment of coronary artery stenosis by coronary flow reserve measurements with transthoracic Doppler echocardiography: comparison with exercise thallium-201 single piston emission computed tomography. *J Am Coll Cardiol.* 2001;37(5):1310-1315.
79. Gadallah S, Thaker KB, Kawanishi D, et al. Comparison of intracoronary Doppler guide wire and transesophageal echocardiography in measurement of flow velocity and coronary flow reserve in the left anterior descending coronary artery. *Am Heart J.* 1998;135(1):38-42.
80. Bedaux WL, Hofman MB, Visser CA, van Rossum AC. Simultaneous noninvasive measurement of blood flow in the great cardiac vein and left anterior descending artery. *J Cardiovascul Magnetic Resonance Official J the Soc Cardiovasc Magnetic Reson.* 2001;3(3):227-235.
81. Burattini R, Sipkema P, van Huis GA, Westerhof N. Identification of canine coronary resistance and intramyocardial compliance on the basis of the waterfall model. *Ann Biomed Eng.* 1985;13(5):385-404.
82. Kresh JY, Fox M, Brockman SK, Noordergraaf A. Model-based analysis of transmural vessel impedance and myocardial circulation dynamics. *Am J Physiol.* 1990;258(2):262-276.
83. Arthurs CJ, Lau KD, Asress KN, Redwood SR, Figueroa CA. A mathematical model of coronary blood flow control: simulation of patient-specific three-dimensional hemodynamics during exercise. *Am J Physiol Heart Circ Physiol.* 2016;310(9):H1242-H1258.

84. Xie X, Wang Y. Flow regulation in coronary vascular tree: a model study. *Plos one*. 2015;10(4). e0125778
85. Moir TW, Debra DW. Effect of left ventricular hypertension, ischemia and vasoactive drugs on the myocardial distribution of coronary flow. 1967;21(1):65-74.
86. Zoghbi GJ, Dorfman TA, Iskandrian AE. The effects of medications on myocardial perfusion. *J Am Coll Cardiol*. 2008;52(6):401-416.
87. Taillefer R, Ahlberg AW, Masood Y, et al. Acute beta-blockade reduces the extent and severity of myocardial perfusion defects with dipyridamole Tc-99m sestamibi SPECT imaging. *J Am Coll Cardiol*. 2003;42(8):1475-1483.
88. Guala A, Leone D, Milan A, Ridolfi L. In silico analysis of the anti-hypertensive drugs impact on myocardial oxygen balance. *Biomech Model Mechanobiol*. 2017;16(3):1-13.
89. Liang F, Guan D, Alastruey J. Determinant factors for arterial hemodynamics in hypertension: theoretical insights from a computational model-based study. *J Biomech Eng*. 2018;140(3):031006.
90. Camici PG, Crea F. Coronary microvascular dysfunction. *N Engl J Med*. 2007;356(8):830-840.
91. Camici PG, D'Amati G, Rimoldi O. Coronary microvascular dysfunction: mechanisms and functional assessment. *Nat Rev Cardiol*. 2014;12(1):48-62.
92. Schwartzkopff B, Motz W, Frenzel H, Vogt M, Knauer S, Strauer BE. Structural and functional alterations of the intramyocardial coronary arterioles in patients with arterial hypertension. *Circulation*. 1993;88(3):993-1003.
93. Rentrop KP, Thornton JC, Feit F, Van Buskirk M. Determinants and protective potential of coronary arterial collaterals as assessed by an angioplasty model. *Am J Cardiol*. 1988;61(10):677-684.
94. Seiler C, Stoller M, Pitt B, Meier P. The human coronary collateral circulation: development and clinical importance. *Eur Heart J*. 2013;34(34):2674-2682.
95. Polese A, De Cesare N, Montorsi P, et al. Upward shift of the lower range of coronary flow autoregulation in hypertensive patients with hypertrophy of the left ventricle. *Circulation*. 1991;83(3):845-853.

How to cite this article: Ge X, Yin Z, Fan Y, Vassilevski Y, Liang F. A multi-scale model of the coronary circulation applied to investigate transmural myocardial flow. *Int J Numer Meth Biomed Engng*. 2018;34:e3123. <https://doi.org/10.1002/cnm.3123>

APPENDIX A

SENSITIVITY OF MODEL SOLUTION TO THE NUMBER OF MYOCARDIAL LAYER DIVISION

While various myocardial layer division strategies have been adopted to model intramyocardial vessels in previous studies, a question remains as to how varying the number of myocardial layer division (N) would affect the outcome of model simulation. To address the issue, we performed a series of numerical tests where N was varied from 3 to 36 at an interval of 3. The baseline vascular resistance and compliance in each myocardial layer were recalculated based on N to ensure that the total baseline resistance and compliance of each intramyocardial vascular subsystem maintain constant despite the variation in N . Herein, to simplify the numerical tests, the vascular resistance and compliance were assumed to be uniformly distributed among myocardial layers.

The sensitivity of model solution to N was evaluated by calculating the normalized root mean square error ($NRMS$) of the LAD flow waves simulated for two adjacent N values.

$$NRMS(N) = \sqrt{\frac{1}{M} \sum_{i=1}^M \left(\frac{y_N^i - y_{N-3}^i}{\bar{y}_{N-3}} \right)^2}, N = 6, 9, \dots, 36, \quad (A1)$$

where M is the total number of numerical time steps in a cardiac cycle; y_N^i, y_{N-3}^i denote the computed flow rates for layer division numbers of N and $N-3$, respectively, with their difference being normalized by the mean flow rate (\bar{y}_{N-3}) corresponding to $N-3$.

Figure A1 illustrates the simulated flow waves in the LAD (panel A), and the changes in $NRMS$ (panel B), mean flow rate in the LAD (panel C), and baseline/effective vascular resistances distal to the LAD (panel C) with N . It is observed that $NRMS$ decreases monotonously with N , falling below 0.02 when N goes larger than 30. Correspondingly, the flow waves converge to a stable waveform, and the mean flow rates gradually approach a constant value. The sensitivity of the simulated flow wave and mean flow rate to N is mediated mainly by the dependence of effective intramyocardial

vascular resistance on N . In the present study, the baseline vascular resistance was defined as the vascular resistance when the vascular wall is unloaded (ie, transvascular pressure = 0 Pa), whereas the effective vascular resistance was derived from the simulated pressure and flow, which is prone to the influence of both hemodynamic conditions and intramyocardial tissue pressure and hence could not be assigned explicitly as a fixed model parameter. Figure A1(D) shows that the effective vascular resistance changes with N despite the fixed baseline resistance. The sensitivity of effective vascular resistance to N is especially high with a small N , but gradually becomes blunt following the increase in N . In other words, the baseline-effective vascular resistance relationship is relatively less affected by an arbitrary choice of N when N is large. In the present study, we chose a layer division number of 31 in consideration of the balance between computational cost and the stability of the relationship between baseline and effective vascular resistances.

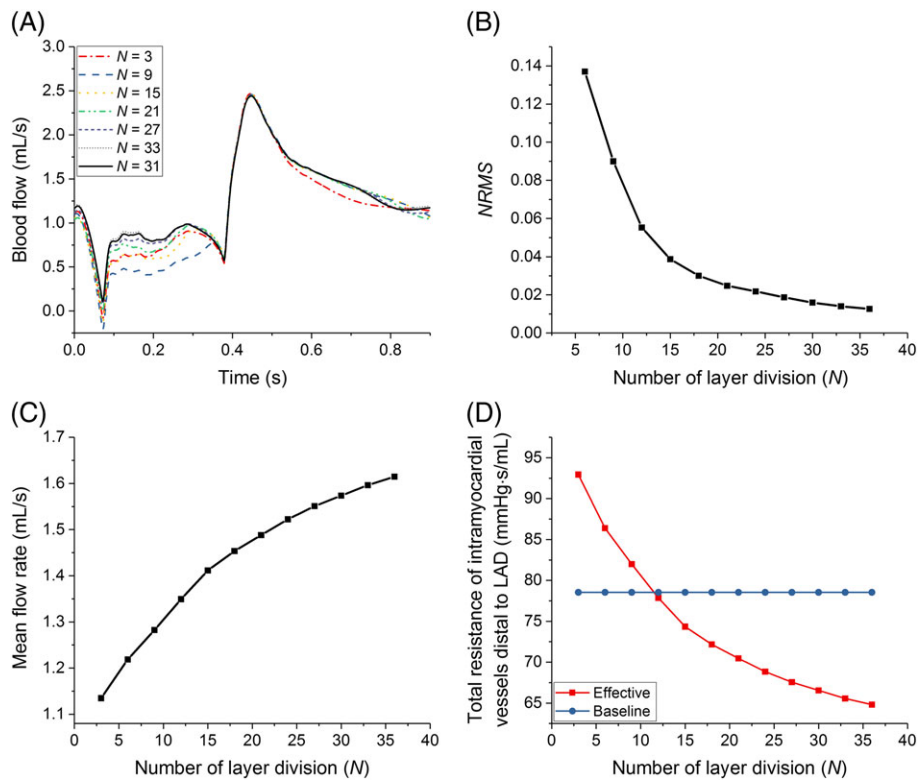


FIGURE A1 Changes in model solutions in response to variations in layer division number (Panel A, blood flow wave in the LAD; Panel B, normalized root mean square error ($NRMS$) of simulated LAD flow waves for two adjacent layer division numbers; Panel C, mean flow rate in the LAD; Panel D, effective and baseline resistances of coronary vessels distal to the LAD)